

## **Geochemical tracing of synoptic scale modern dust transport over the Northeast Arabian Sea during the southwest Monsoon**

**Udisha Singh<sup>1,2</sup>, Suresh, K<sup>3</sup>, Priyesh Prabhat<sup>4</sup>, Waliur Rahaman<sup>4</sup>, Ashwini Kumar<sup>1,2\*</sup>**

<sup>1</sup>CSIR-National Institute of Oceanography, Dona Paula, Goa, India

<sup>2</sup>Academy of Scientific and Innovative Research (AcSIR), Ghaziabad 201002, India

<sup>3</sup>Physical Research Laboratory, Department of Space, Ahmedabad, India

<sup>4</sup>National Centre for Polar and Ocean Research, Ministry of Earth Sciences, Goa, India.

\*Corresponding author: Ashwini Kumar, Geological Oceanography Division

CSIR-National Institute of Oceanography, Dona Paula, Goa-403 004, India

E-mail: ashwinikumarjha@gmail.com, ashwinik@nio.org

Tel: +91 832 2450368, Fax: +91 832 2450602

### **Abstract**

During the Southwest monsoon (SWM), aeolian dust is mainly supplied via wet deposition over the north-eastern Arabian Sea (NEAS). To understand their impact on the biogeochemistry of the Arabian Sea, it is important to identify their sources and characteristics. In this context, wet deposit particulate (WDP) samples were collected at a coastal station (Goa; 15.4° N, 73.8° E) in the NEAS during the SWM for three years. These samples were used to characterize and identify mineral dust sources using mineralogical, elemental, and isotopic (Sr and Nd) signatures. The WDP samples were classified as Beginning of Monsoon (BM, June samples), Mid Monsoon (MM, July- August samples) and End of Monsoon (EM, September samples). Clay mineralogical composition indicate high palygorskite content during BM, which subsequently found to decrease in MM, and almost negligible in EM. However, smectite is highest during MM, with moderate presence of palygorskite during this period. The considerable variation in the relative percentages of clay minerals suggest significant temporal variability in dust sources which is further corroborated by the radiogenic isotopic composition. A strong seasonality in the isotopic composition is observed with  $^{87}\text{Sr}/^{86}\text{Sr}$  ratio being relatively less radiogenic during MM than the BM and highly radiogenic at the EM. Whereas  $\epsilon_{\text{Nd}}$  values show an opposite trend to  $^{87}\text{Sr}/^{86}\text{Sr}$  ratios throughout the monsoon, with more radiogenic  $\epsilon_{\text{Nd}}$  in the MM, and less radiogenic at the EM. End member mixing plot indicate dominant contribution of dust from the Arabian Peninsula (ARB) and Northeast African (NEA) sources during BM and MM, while a shift towards the Thar desert and Southwest Asian (SWA) sources at the EM. Trace elements associated with different sources were quantified and suggest high Fe concentration is associated with NEA dust sources, despite of ARB is the major supplier of aeolian dust to the Arabian Sea.

**Key words:** Mineral dust, Sr-Nd isotopes, Clay mineralogy, Trace Elements, Arabian Sea.

## 1. Introduction

The Arabian Sea (western part of the North Indian Ocean) receive significant amount of aeolian dust from surrounding arid/semi-arid desert regions (Kumar et al., 2020; Suresh et al., 2021a; Aswini et al., 2022; Ramaswamy et al., 2017; Suresh et al., 2021b). The large scale transport of mineral dust, in this basin, is strongly dependent on the prevailing meteorology (Ramaswamy et al., 2017; Aswini et al., 2022) as well as emissions of dust from the surrounding source region (Goudie and Middleton, 2006). During southwest monsoon (SWM) months, dust transport occurs either via higher altitude pathways (between 2-5 Km; Ramaswamy et al., 2017) or carried by episodic wind systems over the Arabian Sea (Suresh et al., 2021a). In addition to predominant SWM winds, regional wind systems such as Shamal wind, Levar wind (Rashki et al., 2019) and Red Sea wind (Patzert et al., 1974) also contribute to dust transport. Summer Shamal and Red Sea winds are northwesterly wind which flow at higher altitude over the Arabian and Nubian desert, respectively, whereas, Levar wind is northerly wind (Alizadeh Choobari et al., 2014) and blows over the southwest Asian region. These regional winds being dry and hot, blow over the dusty areas at a very high speed ( $15-20 \text{ ms}^{-1}$ ) which is strong enough to raise the dust and override the moist and near surface SWM wind in the western Arabian Sea (Ramaswamy et al., 2017).

While the aeolian dust follow high altitude pathways, they get efficiently scavenged via wet deposition (Suresh et al., 2021a). Studies in recent year have emphasized on removal of dust from the troposphere by wet deposition process and highlighted the dominance of wet deposition flux during SWM in contrast to the dry deposition fluxes over the NEAS (Ramaswamy et al., 2017; Suresh et al., 2022). Mineral dust arriving at receptor site (NEAS in this case) are derived from various source regions, get mixed during transport and thus, possibly have varying elemental as well as mineralogical composition (Pease et al., 1998, Usher et al., 2003). This results into different concentration of macro and micro nutrients associated with dust derived from various sources and can impact surface oceanic productivity differently depending on their source region (Guieu et al., 2019). Therefore, characterization of the mineral dust, identification of their sources and concentration of associated nutrients, particularly trace metals, are very crucial to assess their role in impacting surface water biogeochemical processes and improve our understanding of dust-climate interactions.

Considering this, efforts have been made to characterize the mineral dust reaching to the NEAS using geochemical proxies and subsequently used to pin point their sources. Furthermore, attempts have been made to quantify relative contribution of mineral dust from different sources (Kumar et al., 2020; Suresh et al., 2021a). In particular, Suresh et al., 2021b collected wet and dry dust deposits

samples during 2013 and 2012-15 respectively and reported clay mineralogical signatures of dust, its temporal variation and fluxes over the NEAS. The wet deposition fluxes during SWM were observed significantly high in contrast to dry deposition fluxes during rest of the year. However, it is difficult to ascertain the seasonal variability in their source contribution just based on single year data (Suresh et al., 2021a). Moreover, information of trace metal composition and their fluxes associated with aeolian dust transported over the Arabian Sea are limited in the literature. Nair et al. (2006) have reported that western Arabian Sea receives high fluxes of particulates Al, Fe, Mg and Ti through dust bearing north westerlies during SWM. However, the fluxes were found to be peaked in the northern Arabian Sea during both Northeast (NE) and SWM

In addition to dust transport, strong winds during SWM are responsible for coastal (Oman and Somali) (Banse 1987) as well as open ocean upwelling (central Arabian Sea) in the Arabian Sea (Bauer et al. 1991; Kumar et al., 2000; Chowdhury et al., 2021). This results into bringing cold and nutrient rich subsurface water to the coastal surface which further gets advected offshore towards the central Arabian Sea (Morrison et al., 1998) and thus enhances primary productivity in this region (Lee et al., 2000; Barber et al., 2001). However, when advected water towards offshore is not drawn from nutrient rich sub oxic-layers, it always requires an external source of Fe (and other co-limiting nutrients) which can be supplied via aeolian pathway and can significantly modulate primary productivity (Measures and Vink 1999). Several studies over the Arabian Sea, have highlighted role of macro and micro nutrient supply to the surface ocean that can enhance phytoplankton productivity through coastal upwelling during SWM (Rixen et. al., 2000; Barber et. al., 2001) and convective mixing during NE monsoon (Madhupratap et. al., 1996; Prasanna Kumar et. al., 2001). In addition to the supply of nutrients from upwelled water, various studies have emphasized on the significance of nutrients supply to the Arabian Sea via dust deposition (Measure and Vink 1999; Patra et al., 2007; Singh et. al., 2008; Banerjee and Prasanna Kumar, 2014; Guieu et al., 2019). Prasanna Kumar et al. 2010, have reported an annual increase in the chlorophyll a (Ch1 a) due to increase in mineral dust supply in the Arabian Sea. It was reported that although eastern Arabian Sea receives high supply of oceanic nutrients during winter monsoon but high chl a was observed during SWM period and dust input was hypothesized as an important driver (Patra et. al., 2007). Although, role of nutrient rich upwelled water in the Arabian Sea have been discussed in various studies (Brock and McClain, 1992; Naqvi et al., 2010; Prasanna Kumar et al., 2010) but less emphasis was given on the quantification and role of nutrients supplied through aeolian input during SWM., making it difficult to distinguish that which process (upwelled water versus atmospheric input) is potential supplier of nutrients during SWM. Thus, the estimation of trace metal concentrations associated with aeolian dust derived from various sources particularly

during SWM is very essential to constrain and better understand the surface water biogeochemical processes.

In this study, we present Sr and Nd isotopic ratios along with clay minerals as well as major and trace element concentrations measured in the particulate matter collected from wet deposition during SWM months (June, July, August and September) of 2014, 2015 and 2019 over a coastal site in the NEAS. The aim of this study is to provide robust assessment of the seasonality in dust transport and their sources during SWM. Using multiple end-member mixing model, we have attempted to pin point relative contribution of mineral dust from different sources. We have also quantified trace element (TE) concentrations (in particular bioactive TE, e.g. Fe, Cu and Mn) associated with particulates (and/or dust) from different sources.

## **2. Materials and Methods**

### **2.1 Rainwater particulate sampling**

WDP samples were collected on the rooftop of a building located within campus of the National Institute of Oceanography (CSIR-NIO), Goa, (15° 45' N, 73° 80' E) during the southwest monsoon (June-September) period of 2014, 2015 and 2019. The sampling site is located at an altitude of 20 m from sea level and approximately 500 m away from the Arabian Sea. Rain water was collected in a plastic tray (area of 0.81m<sup>2</sup>) which was placed on the rooftop with no interference (tree or building) in near proximity (~ 4 m radius). Collected rainwater was filtered using polycarbonate filter (0.2 µm pore size) to get WDP/dust aerosols. The collected particulates were further dried at room temperature to remove water content from filter. Details of sample collection dates for three years are provided in Table 1. A total of 44 WDP samples were collected and processed (discussed in next section) during the three year of study period. The WDP samples were subjected to analyses of clay minerals, major and trace elements concentration, as well as Sr-Nd isotopic composition.

### **2.2 Analytical methods**

WDP samples were used to prepare oriented glass slides for X-ray diffraction analysis by taking an aliquot of sample collected on polycarbonate filter. Details of sample processing is discussed in Suresh et al., 2021b. Relative composition of clay mineral was quantified by scanning the glass slides using Rigaku® Ultima IV X-Ray Diffractometer with Cu K $\alpha$  radiation at 40kV and 20mA between 3° - 30° 2 $\theta$  at 0.02° 2 $\theta$ /s. The relative percentage of clay minerals are determined semi-quantitatively mainly focusing on major clay minerals which include Illite, smectite, kaolinite, chlorite, and

palygorskite. Weighted peak area of various clay minerals were calculated using correction factors provided by Biscaye [1965].

Approximately 50 mg of WDP samples were taken and leached with deionized water to remove sea salt Sr. The carbonate content in WDP samples were removed using sodium acetate buffered acetic-acid solution (pH = 5) to get silicate fraction. Supernatant fraction kept separately and residue was washed with deionized water twice to remove any excess buffer solution. The remaining residues which were silicate fraction of samples kept for drying at a temperature of 90 °C and acid digested using a mixture of HF-HNO<sub>3</sub> (detailed procedure can be found in Suresh et al, 2021a). Following the same procedure reagent blanks were also processed along with the samples. An aliquot of acid digested samples was kept for major and trace element analyses using ICP-OES and HR-ICPMS respectively (Suresh et al., 2021a). The remaining samples were diluted with 2N HCl and further used to extract pure Sr and Nd using cation exchange column chromatography under clean laboratory condition. The protocol followed for extraction of pure Sr and Nd is detailed in Kumar et al, (2020). Measurement of Sr and Nd isotopic ratios were carried out using multi-collector ICP-MS (Neptune Plus; Thermo Scientific) facility at National Centre for Polar and Ocean Research (NCPOR), Goa, India. While analyzing samples, isotopic composition of known internal standard (NIST SRM987 for Sr and JNdi-1 for Nd) were also measured several times. During these measurement, the average <sup>87</sup>Sr/<sup>86</sup>Sr ratio of internal standard SRM 987 was  $0.710263 \pm 0.000042$  ( $2\sigma$ ,  $n = 10$ ) and JNdi 1 internal standard was  $0.512119 \pm 0.0000056$  ( $2\sigma$ ,  $n=14$ ). Reagent blanks were also analysed along with the samples. Total Sr and Nd blanks were found to be three order of magnitude lower than those present in the WDP samples. Thus, blank correction was not required. The <sup>143</sup>Nd/<sup>144</sup>Nd ratios are expressed in terms of  $\epsilon_{Nd}$ , which is expressed as relative deviation from the Chondrite uniform reservoir (CHUR) ratio of 0.512638 in parts per ten thousand (Jacobsen and Wasserburg, 1980). During trace metal analyses, Rhodium was used as internal standard and a reference material SRM 2711a Montana soil (a certified NIST standard) was also processed and analysed. The recoveries for the reference material was found to be 13% for Cu, 1% for Co, 7% for Mn, 17% for V, 1% for Rb, 18% for Sr, 7% for Cd, 11% for Sm, 13% for Nd, 9% for U and negligible for Th.

### **2.3 Air mass back trajectory analyses and satellite observations**

Winds carrying mineral dust, originating from the source regions during SWM months, take around 5-7 days to reach our sampling site (Suresh et al 2021a), passing over the Arabian Sea, which is also evident from previous studies (Aswini et al., 2020). Thus, the dust fluxes and associated TEs measured at our sampling site can be considered as lower limit of dust concentration. In this study,

HYBRID Single-Particle Lagrangian Integrated Trajectory (HYSPLIT) model was used along with the GDAS meteorological dataset to calculate 7-days air mass back trajectories (AMBT) ending at the sampling site. The HYSPLIT model was run for 168 hours at various altitudes (500-1500 m, 2000-3000 m, and 3000-4500 m) above ground level for the date of sampling. It provides a synoptic picture of dust loaded air mass originating from its source region and its transport towards the sampling location. To spot the active dust source region around the Arabian Sea, Aerosol optical depth (AOD) data (<https://giovanni.gsfc.nasa.gov/giovanni/>) was retrieved over the study area (desert regions and the Arabian Sea) during the sampling period. In addition, CALIPSO (Cloud Aerosol Lidar Infrared Pathfinder Satellite Observations) profiles were also assessed to detect the vertical profile of dust and its presence (available online <https://www-calipso.larc.nasa.gov/>) with the help of satellite passing above or close to the sampling location.

### **3 Results**

#### **3.1 Dust transport identification using AMBT and satellite data**

During SWM, seven days' back trajectories were calculated to track the dust-laden air masses at various altitude along with AOD data and CALIPSO profile, which indicate the presence of the dust. The back trajectories suggest that most of the lower altitude (500-1500 m) wind mass typically represent SWM winds, whereas, at higher altitude (3000-4500m) air masses were mainly arising from the Arabian Peninsula and the Red sea region which represents the summer Shamal wind and Red sea wind at the beginning and the mid- of the monsoon (June to August), respectively (Fig. 1a, 1b, and 1c) (Yu et al., 2017; Ramaswamy et al., 2017; Kumar et al., 2020). At the end of the monsoon (September), the back trajectories were mostly originating from the central Asia/ southwest Asia (SWA) region as well as Thar Desert, representing the Levar winds or the 120 days' wind and thus indicating the changing wind regime (Rashki et al., 2019; Suresh et al., 2021a). Based on analysis of trajectories, all samples collected during SWM have been classified as beginning of monsoon (BM; June), mid of monsoon (MM; July-August) and end of monsoon (EM; September) periods. A representative figure of AOD for the Arabian Sea and dust source region overlaid by AMBTs along with the CALIPSO aerosol sub-type for BM, MM and EM of each sampling year i.e., 2014, 2015 and 2019, are shown in Fig. 1a, 1b and 1c respectively (refer supplementary material S1 for all the other sampling days). AOD images show presence of aerosols over the source region while CALIPSO profiles indicate different aerosol types including mineral dust at different altitudes, above marine atmospheric boundary layer. During BM period of 2014 and 2015, high AOD was observed over the Arabian Peninsula particularly over Oman and Yemen region (Fig. 1a (WDP-14-2) and 1b (WDP-15-4)). The trajectories at higher

altitude were observed to pass over these emission regions with high dust activities and thus, potentially transport the dust to the receptor region i.e. NEAS.

Very high AOD values (higher than 0.8) were seen over the Arabian desert as well as Red Sea coast region during MM period of all study years (Fig. 1a (WDP-14-8), 1b (WDP-15-9) and 1c (WDP-19-5)). Back trajectories at mid and higher altitude also indicate transport of active parcels of air masses (summer Shamal wind and Red sea wind) over these dusty regions and thus may result into higher fluxes of dust reaching to the NEAS during this period. During EM month, the dust sources vary from SWA, northeast Africa (NEA) and the Arabian Peninsula (ARB) region, and large variability is observed in terms of sources impacting dust fluxes over the NEAS. High AOD value was observed over the ARB (Fig 1a. WDP-14-14) which was also complimented with the trajectories at higher altitude originating from this source region. However, during EM period of 2015, AOD profile indicate high dust activity over the ARB as well as over the Thar region (Fig 1b. WDP-15-15) and the wind trajectories were seen to originate from both the emission sources, albeit, at different altitudes. However, CALIPSO profiles clearly provide evidence of dust (Fig. 1b) at different altitudes during 2015. Also, WDP-19-13 (Fig 1c) indicate high AOD value over the ARB as well as over the NEA (coastal Red sea region) and air masses were found to traverse over these regions. Significant amount of dust is evident from the CALIPSO profiles (Fig. 1c) during the EM period of 2019. The dust suspension at various altitude were seen from CALIPSO profile along with their potential sources, however, their relative contribution from different source cannot be decoupled based on the satellite images.

### **3.2 Clay mineralogy**

The clay mineral composition of WDP samples were quantified and their relative percentages as well as ratios are given in Table 1 and their temporal variability is shown in Fig. 2. Mineralogical ratios i.e., illite/kaolinite (I/K), kaolinite/chlorite (K/C), and relative abundance of palygorskite and smectite have been successfully used to characterize atmospheric mineral dust (Claquin et al., 1999; Skonieczny et al., 2013; Kumar et al.; 2020, Suresh et al 2021a). The relative abundance of clay minerals observed in WDP samples were dominated by Illite (17-62%) followed by Smectite (6-42%), Chlorite (9-40%), Palygorskite (8-38%) and Kaolinite (6-20%). An inverse relationship is observed between the abundance of palygorskite and smectite during BM and MM period, excluding the samples collected during EM month (September) for all three years. The average palygorskite content was found relatively high ( $20 \pm 11$  %) for BM samples, which slightly decreases in MM ( $18 \pm 8$ %) and found almost negligible in EM samples (Table 1). However, average smectite is found to be highest during

MM ( $25 \pm 8\%$ ) and relatively low during BM ( $17 \pm 8\%$ ) and EM ( $14 \pm 6\%$ ) period. This is similar to that observed by Suresh et al (2021a) for the WDP samples collected during 2013 SWM period. The I/K values were found to be less than 2 for majority of samples, however, tend to increase during EM samples (ranges between 2.9 to 3.1). In contrast to I/K, no significant variations were observed for K/C ratio during the study period.

### ***3.3 Major and trace elements***

The concentration of major elements (Al, Fe, Ca, Mg and Ti) in WDP samples collected during SWM period of 2014, 2015 and 2019 are given in Table 2b, 2c and 2d respectively. Al is dominant among major elements ranging from 4 to 9% (average 6.6%), followed by Fe (range: 3.4 to 6.5%; average 4.8%). Mg, Ca and Ti ranges between 1 to 4.3%, 0.3 to 1.5%, and 0.4 to 0.7% respectively, similar to dust source region composition reported by Kumar et al. (2020). In this study, Al was used as a tracer of dust for crustal sources (Kumar and Sarin, 2009) and it was found to correlate significantly with Fe and Ti in WDP samples of 2014 ( $r^2 = 0.70; 0.61$ ), and 2015 ( $r^2 = 0.66; 0.63$ ) (Suresh et al., 2022). However, no such significant correlation is observed during 2019 (Supplementary material S2).

During SWM, trace elements (including Fe) associated with dust get deposited in the NEAS which can act as micro-nutrients to the surface waters and thus can impact surface ocean productivity (Jickells et al. 2005; Guieu et al., 2019; Aswini et al., 2022). The composition and concentration of these trace elements (TE) are dependent on the contributions from different active dust sources during various seasons. The trace element (Cu, Co, Mn, V, Rb, Sr, Th, U, Sm, Nd, Cd) composition of WDP for the years 2013 (major elements data is published in Suresh et al., 2021a), 2014, 2015 and 2019 are given in Table 2a, 2b, 2c and 2d respectively. Most of the TEs are correlating well with the Al and Ti except Cu, Co, Rb and Cd for 2014 and 2015 (refer supplementary material S3). However, relatively weak correlation is found for 2019. A very similar correlation was observed for surface soil samples from the source region reported by Kumar et al., (2020). Using the trace metal and Nd isotopic composition, we have attempted to estimate source based TEs contribution over the NEAS and discussed in later section.

### ***3.4 Radiogenic Sr and Nd isotopic composition of WDP***

The  $^{87}\text{Sr}/^{86}\text{Sr}$  ratios in silicate fraction of the WDP dust show large variability with less radiogenic values during MM period for all three years (Fig. 3 and Table 1). The average  $^{87}\text{Sr}/^{86}\text{Sr}$  ratios during BM, MM and EM periods for three years are around 0.7124, 0.7113 and 0.7141 (2014), 0.7136, 0.7100



and 0.7177 (2015), 0.7106 and 0.7126 (2019; no samples collected during BM), respectively. The  $\epsilon_{Nd}$  values also show large variability during three different periods of SWM season for all three years. MM samples display relatively more radiogenic Nd composition (average = -4.5, -3.5 and -4.1 in 2014, 2015 and 2019 respectively) in contrast to BM and EM samples except during 2019 wherein the EM samples have similar signature as of MM period. These isotopic signatures are comparable to that reported by Suresh et al (2021a) (also shown in Fig. 3) revealing a characteristic significant temporal variability during the SWM in the Arabian Sea vis-à-vis at the NEAS.

## **4. Discussion**

### **4.1 Geochemical Characteristics and temporal variability of WDP during SWM**

To characterize dust transported from various emission sources, clay mineralogical and elemental composition (particularly their ratios) have been successfully used in several studies (Stuut et al., 2005; Scheuven et. al., 2013; Abouchami et al., 2013; Seo et al., 2014; Xu et al., 2015; Zhao et al., 2015; Kumar et al. 2020, Suresh et al., 2021). The Fe/Al and Ti/Al ratios varied from 0.62-0.79 and 0.07-0.09 (WDP 2014), 0.60-1 and 0.06-0.09 (WDP 2015) and 0.7-1.1 and 0.09-0.12 (WDP 2019) respectively. The Fe/Al ratio of these samples are (range: 0.6-1) enriched in comparison to the UCC value of 0.44 as reported by McLennan, 2001. The observed value for 2014, 2015 and 2019 were comparable to the WDP samples collected at the NEAS during the SWM season of 2013 (Suresh et. al., 2021b) (Fe/Al 0.65-1.08 and Ti/Al 0.06-0.10). While, large range is observed in these ratio, no characteristic signature is found for BM, MM and EM samples. The average value of these ratios (Fe/Al and Ti/Al; for all three years) in each period i.e. BM, MM and EM is found to be ( $0.68 \pm 0.03$ ;  $0.07 \pm 0$ ), ( $0.77 \pm 0.1$ ;  $0.09 \pm 0.02$ ) and ( $0.76 \pm 0.15$ ;  $0.08 \pm 0.02$ ), respectively. Chiapello et al. 1997 and Zhang et al. 1996, used similar approach to characterize dust source regions in Africa and Asia, respectively. Also, Kumar and Sarin 2009 and Gaonkar et al., 2020 characterize dust over Indian region using major elements ratio. However, no significant temporal variability is observed in our data and thus, these ratios have limitations to characterize a particular signature of dust sources and/or cannot be used as a tracer for source identification, although similar approaches have been successful elsewhere.

Clay minerals relative abundance and their ratios have been used to characterize the mineral dust and their corresponding sources, which are basically weathered material of pre-existing minerals from parent rock and their origin and evolution largely depends on various climatic, geological and weathering environments (Galan et. al., 2006, Chamley et. al., 1989). The average I/K (for three years) ratio shows almost similar values for BM ( $1.85 \pm 0.68$ ) and MM ( $1.80 \pm 0.65$ ) samples, however,

relatively higher values were observed for those samples collected in the EM ( $3.2\pm 1.01$ ) months. Majority of samples (around 60 %) in BM and MM months show low I/K values (less than 1.5; Fig. 2a), similar to those reported by Suresh et al. (2021a). The I/K ratio for the ARB ranges from 1.0-1.3, whereas it was observed to be higher for SWA (1.8 – 7.3) and Thar desert (1.0 – 8.2) (Kumar et al., 2020). Thus, an increase in the I/K ratio suggest change in dust sources from the ARB to SWA and the Thar Desert. Similar to I/K, no significant change is found in average K/C values for BM ( $0.81\pm 0.19$ ) and MM ( $0.87\pm 0.25$ ) samples (Fig. 2a). However, relatively lower values were seen for EM ( $0.70\pm 0.10$ ) samples which is similar to those reported for SWA ( $0.67\pm 0.12$  and 0.70) by Suresh et al (2021a) and Svensson et al. (2000), respectively.

Palygorskite and Smectite are important clay minerals prominently found in the ARB and NEA sources regions. Smectite is reported to be high with moderate to less palygorskite in the NEA region (Gulf of Aden) due to weathering of basalts in the Afar volcanic region and also from the Arabian Nubian shield granitoids (Red Sea region) (Rojas et al., 2019). Palygorskite is a fibrous clay mineral which is formed in the semi-arid and saline environment such as in sabkha and wadi deposits in the Arabia and also found in NEA desert (Debrabant et al., 1991). Their relative abundance has been successfully used to identify sources of mineral dust over the Arabian Sea (Kumar et al., 2020; Suresh et al., 2021a). During BM (of 2014 and 2015), palygorskite content is relatively high, which subsequently found to decrease in MM, including 2019 samples and almost negligible in EM samples (Fig. 2b). The P/I value averaged around 0.85 for all three periods (BM:  $0.87\pm 0.66$ ; MM:  $0.82\pm 0.47$  and EM:0.86) with insignificant variation, particularly during 2014 and 2019. However, relatively higher values were shown by 2015 samples wherein, BM samples have average P/I of  $1.27\pm 0.65$  falling in the range of P/I value reported for dust samples sourced from the ARB (Kumar et al., 2020). While there were no significant variations in P/I ratios, we witnessed an enhanced contribution of Smectite abundance in MM (9 to 42 %) in contrast to BM (range: 9 to 29 %) with negligible contribution during EM for all three years. This is also evident from higher S/P ratio during MM ( $1.85\pm 1.24$ ) in comparison to BM ( $1.03\pm 0.62$ ). These observations suggest an increased contribution of dust from the NEA sources during the peak monsoon period in SWM. Rojas et. al., (2018) have reported higher smectite content (50-70%) with lesser quantity of palygorskite (5-20%) in the clay size fraction of the core collected from the Gulf of Aden (near Horn of Africa). Similarly, high smectite (55-80%) with less palygorskite content (5-10%) was observed from another core from Red sea region (Rojas et. al., 2019). These studies indicate that Horn of Africa and Gulf of Aden could provide relatively higher smectite than palygorskite which is also observed in our WDP samples particularly during MM.

Radiogenic Sr and Nd isotopic composition measured in the WDP samples have been used for characterization to further assess their temporal variability and identify potential dust sources contributing to the NEAS vis-à-vis the Arabian Sea. Highly radiogenic Sr isotopic composition is displayed by BM samples which tend to decrease during MM period and subsequently found to increase in the EM period. This trend is seen in all three years of the study period. Average  $^{87}\text{Sr}/^{86}\text{Sr}$  during BM period of 2014 and 2015 were observed to be  $0.7124 \pm 0.0009$ , and  $0.7136 \pm 0.0031$  respectively. However, during MM period of 2014, 2015 and 2019, the  $^{87}\text{Sr}/^{86}\text{Sr}$  ratios were seen to average around  $0.7113 \pm 0.0011$ ,  $0.7122 \pm 0.0010$  and  $0.7116 \pm 0.0006$ ., respectively. Although, the number of samples collected in the EM period was less, but the average  $^{87}\text{Sr}/^{86}\text{Sr}$  value found to be  $0.7141 \pm 0.0008$ ,  $0.7185 \pm 0.0011$  and  $0.7126 \pm 0.0001$  respectively. The  $\epsilon_{\text{Nd}}$  values shows an opposite trend with highly radiogenic values during MM period and relatively lower values in the BM and EM periods. The  $\epsilon_{\text{Nd}}$  values during MM period of 2014, 2015 and 2019 were found to vary from  $-3.0$  to  $-5.7$ ,  $-0.6$  to  $-5.2$  and  $-2.5$  to  $-5.3$ , respectively. However, the average Nd isotopic composition show less radiogenic signatures during BM and EM periods (Table-1 and Fig. 3). The isotopic signature of majority of the MM samples (See Table 1) are significantly different than those reported for the ARB and SWA by Kumar et al. (2020), suggesting potential contribution from a completely different dust source contributing to the Arabian Sea during the SWM. The arid/semi-arid region in the NEA could be a potential source for dust supply which possibly gets carried along with Findlater Jet, augmented by Red sea winds during SWM (Ramaswamy et al., 2017). The NEA desert region is mainly composed of Cenozoic alkali basalts, acting as major source of the sediments in the Afar region (located in the parts of Ethiopia, Eritria and Djibouti) with a relatively more radiogenic  $\epsilon_{\text{Nd}}$  values (0 to +10) and lower  $^{87}\text{Sr}/^{86}\text{Sr}$  ratios (0.703 to 0.705) (Betton and Civetta, 1984; Teklay et al., 2009; Ayalew et al., 2018). The characteristic isotopic signature of WDP dust collected from a coastal site in the NEAS indicates a similar type of dust transported over the Arabian Sea during SWM period. Based on the three-year data, a significant temporal variability can be seen in the dust characteristics. This variability is majorly governed by the dust emission activity as well as conducive meteorological factors, which include wind pattern, over the Arabian Sea.

#### **4.2 Identifying potential sources of dust using multi proxy approach**

The limited availability of Sr and Nd isotope database of soil or sediments from the surrounding arid and semi-arid sources makes it difficult to exactly pinpoint the provenance of dust reaching to the Arabian Sea. Though studies have been attempted to characterize the dust provenance over the western Arabian Sea using Sr and Nd isotopic composition (Jung et. al., 2004; Palchan et. al., 2013; Rojas et.

al., 2019) yet the data are very limited particularly over the NEAS (Kumar et al., 2020; Suresh et. al., 2021a). In this study, we used published Sr and Nd isotopic data (Sirocko 1995; Tripathi et al., 2004; Ferrat et. al., 2011; Ayalew et. al., 2018) from the possible source regions to trace the provenance of the WDP collected during SWM period. The transport of dust and its deposition to the surface water of the Arabian Sea is largely controlled by the prevailing wind system over the source region. Recent studies have discussed about major sources supplying dust to the NEAS which include ARB, NEA, SWA and Thar desert (Ramaswamy et. al., 2017; Kumar et. al., 2020; Suresh et. al., 2021a). During SWM, the dominant wind system over the north Indian ocean are SWM winds, however the dust from the sources are mainly uplifted by strong regional wind systems active over these dry or semi-arid regions such as Summer Shamal, Levar and Red sea winds which override SWM wind and thus result in transport of dust to the Arabian Sea (as discussed previously). The WDP (three years' data along with published 2013 data from Suresh et al., 2021a) Nd and Sr isotopic datasets are plotted in Fig. 4 along with four end members (ARB, NEA, SWA, and Thar desert) characterizing the main potential source areas. The end member isotopic composition (Sr and Nd) and concentration are provided in Table 3 which are based on the data available in literature (Sirocko, 1995; Tripathi et al., 2004; Ferrat et al., 2011; Ayalew et al., 2018; Kumar et al., 2020). As the samples were classified as BM, MM, and EM (mentioned in section 3.1), the source apportionment of the WDP samples are discussed based on this classification.

It was observed that during BM period, majority of the samples lie on or the edge of ARB end member (Fig. 4) with more radiogenic  $^{87}\text{Sr}/^{86}\text{Sr}$  (average:  $0.7125 \pm 0.0019$ ) and less radiogenic  $\epsilon_{\text{Nd}}$  (average:  $-5.4 \pm 1.0$ ). However, few samples found to lie towards NEA field and based on mixing equation (Faure and Mensing 2005), ~10-20% contribution from NEA sources were observed. This result was also supported by mineralogy data where we observed that the samples which are falling in the ARB region have high palygorskite (average:  $29\% \pm 12\%$ ) and less smectite content (average:  $15\% \pm 7\%$ ) whereas those samples having ~10-20% contribution from NEA sources have approximately the same palygorskite (average:  $20\% \pm 11\%$ ) and smectite (average:  $21\% \pm 9\%$ ) abundance. The AOD profile also suggest high aerosol activity over ARB region particularly during BM period and its transport to the NEAS is corroborated with back-trajectory analysis which indicate transport of dust at higher altitude (2500 m). The retrieved CALIPSO profiles (closest overpass to the sampling site) available during the sampling period also indicate the presence of mineral dust over the NEAS.

During MM period, majority of data falls near and/ or on the mixing line between ARB and NEA (Fig. 4) with less radiogenic  $^{87}\text{Sr}/^{86}\text{Sr}$  (average:  $0.7116 \pm 0.0010$ ) and more radiogenic  $\epsilon_{\text{Nd}}$  (average: –

4.1 ± 1.1). Though majority of the samples during this period, found to be close to NEA end member yet few samples falls in ARB field (WDP 14- 5, 9 10, 13; WDP 15-8, 14, and WDP 19-3). Based on the end member mixing equation between ARB and NEA, we observed that during MM period the contribution from NEA sources vary considerably and increases as much as 30-40% (WDP 14-8 and 11, WDP 15-6) to 50-60% (WDP 15-10). This increase in the contribution from NEA is also well documented with highly radiogenic  $\epsilon_{Nd}$  value of -3.0 (WDP 14-8), -3.4 (WDP 14-11), -1.9 (WDP 15-6), and -0.6 (WDP 15-10) indicating dust reaching to the NEAS consist of mix contribution of sources located in the ARB as well as NEA. Also, the smectite content in the samples tending towards NEA end member was observed to have relatively higher smectite (average: 28% ± 10%) with moderately low palygorskite content (average: 18% ± 7%) than those samples falling particularly in ARB field with less smectite content (21% ± 6%) and high palygorskite abundance (average: 24 ± 8%). These isotopic and mineralogical data indicate that, although ARB is a major contributor of dust to the Arabian Sea yet contribution from NEA increases significantly during MM period. Similar results were observed by Suresh et al., (2021a) during SWM months of 2013. This interpretation is also well supported with the satellite retrieved CALIPSO and AOD profile indicating high dust activity over ARB as well as Red sea region. The back trajectory analysis during this period indicate active air masses at different altitude (between 2000 and 4500 m) which may result into mixing of dust while its transport from the ARB and NEA to the NEAS.

The data for EM period falls near SWA and Thar desert isotopic field as well as ARB and NEA end members (Fig. 4), indicating large variability in the dust sources during EM period. As compared to BM and MM, a gradual increase in  $^{87}Sr/^{86}Sr$  ratio (average: 0.7153 ± 0.0028) was observed with a decrease in  $\epsilon_{Nd}$  value (average: -6.4 ± 2.4) during this period. Three of these EM samples (WDP 14-14, WDP 19-14 and WDP 15-15) fall on or near ARB field with one of the samples having relatively high palygorskite content (~25% in WDP 19-14). Whereas out of the two samples (WDP 14-15 and WDP 19-13) which lie towards NEA region, WDP 19-13 contains high smectite (~ 21%), indicating their occurrence from the horn of Africa. Though high AOD was observed over ARB as well as NEA for WDP 19-13 (Fig. 1c) yet air-masses were found to traverse over the NEA supporting dust transport from this region. Few WDP samples (WDP 15-16, WDP 13- 15 and WDP 13- 16) collected during EM lie close to the mixing line between ARB and Thar desert with one of the samples falling in the SWA field (WDP 13-14). The sample falling in SWA source has high Illite (~46%) and chlorite (~17%) content with less palygorskite (~13%) and smectite (~16%) abundance. Whereas the samples falling towards Thar desert source have high illite (average: 53% ± 3%) and chlorite (average: 32% ± 7%) abundance with negligible contribution of palygorskite and smectite similar to those reported by

Tripathi et al., (1997). This suggest the contribution of SWA and the Thar increases towards the EM with episodic contributions from the ARB.

We have further investigated variability in dust sources using  $\epsilon_{Nd}$  values with relative smectite content (Fig. 5) which tend to correlate significantly ( $r = 0.63$ ;  $p < 0.005$ ). It was observed that during MM,  $\epsilon_{Nd}$  value tends to become more radiogenic (ranges from -0.6 to -5.7) which is supported with a continuous increase in smectite percentages (ranges from 9 to 56 %). Whereas during BM, the  $\epsilon_{Nd}$  value became less radiogenic (ranges from -4.3 to -7.2) with a decrease in smectite percentages (ranges from 9-32%). We observed almost negligible contribution of smectite during EM samples (except few samples which have more radiogenic  $\epsilon_{Nd}$  value) with unradiogenic  $\epsilon_{Nd}$  value (ranges from -7.1 to -9.0). Smectite is basically a weathering product of volcanic rocks and its abundance during MM indicates a basaltic origin probably transported from Afar region (Van Den Eeckhaut et al., 2009). Also, reduction in smectite percentage and the associated less radiogenic  $\epsilon_{Nd}$  value indicate the source from ARB which is well supported with the increase palygorskite percentage during BM (Fig. 2b). Rojas et al, 2018 have also reported high smectite abundance (ranges from 50-80%) from the cores sampled in Gulf of Aden and Red Sea region where they observed a positive correlation between  $\epsilon_{Nd}$  values and Smectite content. This observation supports our inference of increased contribution of the NEA sources during MM period over the Arabian Sea.

### 4.3 Variation in micronutrients associated with different dust sources

We have attempted to assess the variation of micronutrients (TEs particularly Cu, Mn and Fe) concentration in relation to different dust sources identified using Nd isotopic composition (being more robust tracer; Kumar et al., 2020). These bioactive nutrients (Cu, Mn and Fe) can be utilized by phytoplankton in various biological processes which can modulate the productivity and hence the biogeochemical cycle (Panda et al., 2022). Average micronutrients concentration (in ppm) against average  $\epsilon_{Nd}$  values for four identified dust source regions which include ARB, mix of ARB and NEA, the Thar desert and SWA (only one sample identified for SWA source) are shown in Fig. 6. Since the trace element concentration was measured in silicate fraction therefore the concentration of these elements are assumed to be sourced primarily from mineral dust. We observed large variability in TEs concentrations, which may be due to limited set of data available from each source. The variation in Cu concentration (in ppm) is found to be comparatively higher in the ARB (average:  $102 \pm 44$ ) than mix of ARB and NEA (average;  $92 \pm 22$ ) and Thar desert region (average;  $98 \pm 7$ ), however, extremely high for the SWA (236 ppm) derived dust (Fig 6 a). This is very high in contrast to the soil/sediment samples collected over Iran region ( $54 \pm 18$  ppm) reported by Kumar et., al (2020). The observed Cu

concentration in ARB, NEA and Thar desert sources were almost twice of data reported from the surface sediment of core sample near Oman (53 ppm), and Gulf of Aden (51 ppm) (Sirocko et. al., 2000) and soil samples from the Thar region (average:  $70 \pm 34$  ppm) (Kumar et. al., 2020).

Mn is observed to be relatively higher in samples sourced from ARB (average:  $743 \pm 167$  ppm) and mix of ARB and NEA (average:  $806 \pm 138$  ppm) than those derived from the Thar desert ( $586 \pm 85$  ppm) and SWA sources (511 ppm) (Fig. 6 b). The observed Mn concentration in ARB is comparable to the data reported by Sirocko et. al., 2000 over a surface sediment of core sample (650 ppm). However, the reported Mn concentration is much higher over the Gulf of Aden (1880 ppm) and main Ethiopian rift (average:  $2112 \pm 1389$ ) (Sirocko et. al., 2000; Ayalew et. al., 2018) than those observed for the mix of ARB and NEA source, suggesting the dilution in Mn concentration due to contribution from Mn depleted ARB source. A large variability in Mn concentration is also reported by Kumar et. al., (2020) in silicate fraction of soil samples (ranges from 688 to 1639) and Yadav and Rajamani, (2003) in free fall samples (775 ppm) collected over the Thar desert region, indicating contribution from various local sources within Thar region. The average Fe concentration is shown (Fig. 6 c) to be relatively high in mix source of ARB and NEA (average:  $49116 \pm 8315$ ) than ARB (average:  $45091 \pm 7326$  ppm) and Thar desert (average:  $44968 \pm 4572$  ppm) sources. However, a comparatively high Fe concentration (55000 ppm) was observed from the SWA source. Based on mean value we can interpret that the concentration of Fe relatively increases when the dust derives from the NEA sources which are dominated by basaltic rock rich in Fe content (Ayalew et. al., 2018). These observations imply that different sources supply varied amounts of micronutrients during the SWM, which eventually reaches to the Arabian Sea and can impact surface ocean biogeochemistry.

#### **4.4 Implication for micronutrient supply to the Arabian Sea**

The nutrient supply to the Arabian Sea during SWM is associated with upwelling as well as atmospheric deposition of mineral dust. Although, both processes play a significant role impacting surface ocean biogeochemistry yet upwelling driven nutrient supply is largely limited to the coastal region. However, supply of nutrients via dust deposition reaches to the remote ocean as well, suggesting atmospheric deposition as a major contributor of nutrients particularly in the open ocean region. A very recent study on a sediment core offshore Saurashtra, delineate an enhanced aeolian contribution from ARB and NEA due to weakening of SWM throughout mid and late Holocene contrary to high fluvial supply due to stronger monsoon during early Holocene. Additionally, elemental (major and trace elements) concentration remained low throughout the early Holocene, however, an increasing trend in the elemental composition of sediment core was observed during mid

Holocene which became stable at the late Holocene indicating high nutrients flux associated with enhanced dust supply during this period. which could impact palaeo-productivity and thus biogeochemical cycle (Rahaman et al., 2023).

Various studies have highlighted that atmospheric deposition of mineral dust provide essential macro and micro-nutrient to the Arabian Sea during SWM (Wiggert and Murtugudde, 2007; Ramaswamy et al., 2017; Panda et al., 2022) yet it is difficult to assess which source is particularly important in terms of nutrients supply during this period. Here we quantified the relative proportion of nutrients associated with individual dust sources using mixing model (supplementary material S4). Our data indicate that Cu, Mn and Fe are being supplied continuously throughout the monsoon from various identified dust sources (ARB, mix of ARB and NEA, and the Thar desert), but the concentration of Fe was observed to be particularly high when the dust derived from ARB as well as NEA. Through mixing plot, it has been observed that both the dust sources i.e. ARB and NEA are active during MM period. High dust flux attributed to the heavy precipitation and strong dust laden Summer Shamal and Levar wind was also reported by Suresh et al., (2022) during MM. The increase input of Fe concentration associated with high dust flux during MM can modulate the primary productivity in the Arabian Sea. Based on the satellite data and modeling studies, an increase in phytoplankton productivity was observed with the passage of dust storm over the central Arabian Sea (Banerjee and Prasanna Kumar, 2014). Also, Guieu et al., (2019) have observed that P and Fe deposition peaks during June and July over the Arabian Sea demonstrating that atmospheric deposition plays a significant role in carbon fixation over this region. They have also reported that, although upwelled water near ARB coast is rich in nutrients yet the limitation of Fe could reduce the primary productivity by > 50%. Therefore, the atmospheric deposition of Fe is required to fuel the biological productivity in this region. Thus our study emphasized, though ARB act as a major supplier of atmospheric dust to the Arabian Sea yet NEA is playing a key role through increase supply of Fe associated with increase dust deposition during MM which can ultimately impact the surface ocean biogeochemistry of the Arabian Sea. The TEs dataset associated with dust sources reported in this study is a step forward to constrain supply of these key micro-nutrients to the Arabian Sea.

## **5. Summary and Conclusion**

In his study, we present the geochemical characteristics of wet deposited dust particles collected from a coastal site in the NEAS to understand provenance of aeolian dust and quantify bioactive trace element concentration associated with mineral dust during the SWM. Major outcome of this study are:



1. Palygorskite, Smectite, Kaolinite (K), Illite (I) and Chlorite (C) are the major clay minerals identified during the study period. I/K ratios show a gradual increase from BM to MM, with highest values at the EM suggesting contribution from SWA and Thar desert. However, no significant variation was observed for K/C ratios.
2. Palygorskite content is high during BM, which subsequently found to decrease in MM and almost negligible in EM samples, whereas, smectite is found to be highest during MM except for few samples collected during the SWM period with moderate presence of palygorskite.
3. A very significant variability is observed in Sr-Nd isotopic composition of aeolian dust with relatively more radiogenic  $^{87}\text{Sr}/^{86}\text{Sr}$  ratios during BM and EM and less radiogenic during MM. Whereas, the  $\epsilon_{\text{Nd}}$  values show an opposite trend to that of the  $^{87}\text{Sr}/^{86}\text{Sr}$  ratios throughout the monsoon, with more radiogenic  $\epsilon_{\text{Nd}}$  in the MM, and less radiogenic at the EM.
4. End member mixing plot indicate dominant contribution from ARB and NEA during BM and MM, while a shift towards SWA and Thar dust sources were seen at the EM period.
5. These inferences from clay mineralogy and radiogenic isotope tracers were corroborated by satellite images (CALIPSO and AOD) as well as back-trajectory analyses
6. Higher concentration of Fe was found to be associated with the NEA sourced dust, however, ARB is found to be major supplier of mineral dust to the Arabian Sea during the SWM months.

This 3-year geochemical data set on dust characteristics and their sources via wet deposition is filling a large research gap in the understanding of dust and trace element cycling over the Arabian Sea. Furthermore, the geochemical data will be useful for the assessment of marine sedimentary records to better infer mineral dust related processes in the past and its role in the paleo-productivity.

#### **Acknowledgment:**

Funding for this research is supported by CSIR CLICNIO (MLP1802). Ashwini Kumar thanks for partial fund support from the Department of Science and Technology, Govt. of India, under the Core research Grant (File no. CRG/2021/003307). Udisha Singh, and K Suresh thanks the Department of Science and Technology, Govt. of India, INSPIRE Research Fellowship (IF180350) and (IF140405) respectively. We thank Mr. Robin for support during analyses of major and trace elements and Mr Girish A. Prabhu for assistance in clay minerals analyses. We gratefully acknowledge the NOAA Air Resources Laboratory (ARL) for the provision of the HYSPLIT transport and dispersion model (<http://www.ready.noaa.gov>) used in this publication.

## References

- Abouchami, W., Nathe, K., Kumar, A., Galer, S. J., Jochum, K. P., Williams, E., ... & Andreae, M. O. (2013). Geochemical and isotopic characterization of the Bodel Depression dust source and implications for transatlantic dust transport to the Amazon Basin. *Earth and Planetary Science Letters*, 380, 112-123.
- Alizadeh-Choobari, O., Zawar-Reza, P., & Sturman, A. (2014). The “wind of 120 days” and dust storm activity over the Sistan Basin. *Atmospheric research*, 143, 328-341.
- Arimoto, R. I. C. H. A. R. D. (1989). Concentrations, sources and air-sea exchange of trace elements in the atmosphere over the Pacific Ocean. *Chemical Oceanography*, 10, 107-149.
- Aswini, M. A., Kumar, A., & Das, S. K. (2020). Quantification of long-range transported aeolian dust towards the Indian peninsular region using satellite and ground-based data-A case study during a dust storm over the Arabian Sea. *Atmospheric Research*, 239, 104910.
- Aswini, M. A., Tiwari, S., Singh, U., Kurian, S., Patel, A., Gunthe, S. S., & Kumar, A. (2022). Aeolian Dust and Sea Salt in Marine Aerosols over the Arabian Sea during the Southwest Monsoon: Sources and Spatial Variability. *ACS Earth and Space Chemistry*, 6(4), 1044-1058.
- Ayalew, D., Jung, S., Romer, R. L., & Garbe-Schonberg, D. (2018). Trace element systematics and Nd, Sr and Pb isotopes of Pliocene flood basalt magmas (Ethiopian rift): A case for Afar plume-lithosphere interaction. *Chemical Geology*, 493, 172-188.
- Badarinath, K. V. S., Kharol, S. K., Kaskaoutis, D. G., Sharma, A. R., Ramaswamy, V., & Kambezidis, H. D. (2010). Long-range transport of dust aerosols over the Arabian Sea and Indian region—A case study using satellite data and ground-based measurements. *Global and Planetary Change*, 72(3), 164-181.
- Banerjee, P., & Prasanna Kumar, S. (2014). Dust-induced episodic phytoplankton blooms in the Arabian Sea during winter monsoon. *Journal of Geophysical Research: Oceans*, 119(10), 7123-7138.
- Banse, K., 1987. Seasonality of phytoplankton chlorophyll in the central and northern Arabian Sea. *Deep Sea Res. Part A* 34 (5–6), 713–723. [https://doi.org/10.1016/0198-0149\(87\)90032-X](https://doi.org/10.1016/0198-0149(87)90032-X).
- Barber, R.T., Marra, J., Bidigare, R.C., Codispoti, L.A., Halpern, D., Johnson, Z., Latasa, M., Goericke, R., Smith, S.L., 2001. Primary productivity and its regulation in the Arabian Sea during 1995. *Deep Sea Res. Part II* 48 (6–7), 1127–1172. [https://doi.org/10.1016/S0967-0645\(00\)00134-X](https://doi.org/10.1016/S0967-0645(00)00134-X).
- Bauer, S., Hitchcock, G.L., Olson, D.B., 1991. Influence of monsoonally-forced Ekman dynamics upon surface layer depth and plankton biomass distribution in the Arabian Sea. *Deep Sea Res. Part A* 38 (5), 531–553. [https://doi.org/10.1016/0198-0149\(91\)90062-K](https://doi.org/10.1016/0198-0149(91)90062-K)
- Betton, P. J., & Civetta, L. (1984). Strontium and neodymium isotopic evidence for the heterogeneous nature and development of the mantle beneath Afar (Ethiopia). *Earth and planetary science letters*, 71(1), 59-70.

- Bory, A. J. M., Biscaye, P. E., & Grousset, F. E. (2003). Two distinct seasonal Asian source regions for mineral dust deposited in Greenland (NorthGRIP). *Geophysical research letters*, 30(4).
- Boyd, P. W., Wong, C. S., Merrill, J., Whitney, F., Snow, J., Harrison, P. J., & Gower, J. (1998). Atmospheric iron supply and enhanced vertical carbon flux in the NE subarctic Pacific: is there a connection?. *Global Biogeochemical Cycles*, 12(3), 429-441.
- Brock, J. C., & McClain, C. R. (1992). Interannual variability in phytoplankton blooms observed in the northwestern Arabian Sea during the southwest monsoon. *Journal of Geophysical Research: Oceans*, 97(C1), 733-750.
- Caquineau, S., Gaudichet, A., Gomes, L., Magonthier, M. C., & Chatenet, B. (1998). Saharan dust: Clay ratio as a relevant tracer to assess the origin of soil-derived aerosols. *Geophysical research letters*, 25(7), 983-986.
- Chamley, H., & Lille, U. (1989). Clay mineralogy.
- Chiapello, I., Bergametti, G., Chatenet, B., Bousquet, P., Dulac, F., & Soares, E. S. (1997). Origins of African dust transported over the northeastern tropical Atlantic. *Journal of Geophysical Research: Atmospheres*, 102(D12), 13701-13709.
- Chowdhury, M., Biswas, H., Mitra, A., Silori, S., Sharma, D., Bandyopadhyay, D., ... & Narvekar, J. (2021). Southwest monsoon-driven changes in the phytoplankton community structure in the central Arabian Sea (2017–2018): After two decades of JGOFS. *Progress in Oceanography*, 197, 102654.
- Das, S., Dey, S., Dash, S. K., Giuliani, G., & Solmon, F. (2015). Dust aerosol feedback on the Indian summer monsoon: Sensitivity to absorption property. *Journal of Geophysical Research: Atmospheres*, 120(18), 9642-9652.
- Debrabant, P., Krissek, L., Bouquillon, A., & Chamley, H. (1991). Clay mineralogy of Neogene sediments of the western Arabian Sea: mineral abundances and paleoenvironmental implications. In *Proceedings of the ocean drilling program, Scientific Results* (Vol. 117, pp. 183-186). College Station, TX: Ocean Drilling Program.
- Duce, R. A., & Tindale, N. W. (1991). Chemistry and biology of iron and other trace metals. *Limnol. Oceanogr*, 36(8), 1715-1726.
- El-Askary, H., Gautam, R., Singh, R. P., & Kafatos, M. (2006). Dust storms detection over the Indo-Gangetic basin using multi sensor data. *Advances in Space Research*, 37(4), 728-733.
- Faure, G., & Mensing, T. M. (2005). *Principles and applications* (p. 897). John Wiley & Sons, Inc.
- Ferrat, M., Weiss, D. J., Strekopytov, S., Dong, S., Chen, H., Najorka, J., ... & Sinha, R. (2011). Improved provenance tracing of Asian dust sources using rare earth elements and selected trace elements for palaeomonsoon studies on the eastern Tibetan Plateau. *Geochimica et Cosmochimica Acta*, 75(21), 6374-6399.
- Galán, E. (2006). Genesis of clay minerals. *Developments in clay science*, 1, 1129-1162.

- Gaonkar, C. V., Kumar, A., Matta, V. M., & Kurian, S. (2020). Assessment of crustal element and trace metal concentrations in atmospheric particulate matter over a coastal city in the Eastern Arabian Sea. *Journal of the Air & Waste Management Association*, 70(1), 78-92.
- Garrison, V. H., Shinn, E. A., Foreman, W. T., Griffin, D. W., Holmes, C. W., Kellogg, C. A., ... & Smith, G. W. (2003). African and Asian dust: from desert soils to coral reefs. *BioScience*, 53(5), 469-480.
- Goudie, A. S., & Middleton, N. J. (2006). *Desert dust in the global system*. Springer Science & Business Media.
- Grousset, F. E., & Biscaye, P. E. (2005). Tracing dust sources and transport patterns using Sr, Nd and Pb isotopes. *Chemical Geology*, 222(3-4), 149-167.
- Guieu, C., Al Azhar, M., Aumont, O., Mahowald, N., Lévy, M., Éthé, C., & Lachkar, Z. (2019). Major impact of dust deposition on the productivity of the Arabian Sea. *Geophysical Research Letters*, 46(12), 6736-6744.
- Guo, J., Pereyra, Y., Ma, L., Gaillardet, J., Sak, P. B., & Bouchez, J. (2017, December). Using Nd and Sr isotopes to trace dust and volcanic inputs to soils on French Guadeloupe Island. In *AGU Fall Meeting Abstracts* (Vol. 2017, pp. PP21B-1255).
- Jabłońska, M., Janeczek, J., & Smieja-Król, B. (2021). The impact of ambient atmospheric mineral-dust particles on the calcification of lungs. *Minerals*, 11(2), 125.
- Jickells, T. D., An, Z. S., Andersen, K. K., Baker, A. R., Bergametti, G., Brooks, N., ... & Torres, R. (2005). Global iron connections between desert dust, ocean biogeochemistry, and climate. *science*, 308(5718), 67-71.
- Johnson, M. S., Meskhidze, N., Kiliyanpilakkil, V. P., & Gasso, S. (2011). Understanding the transport of Patagonian dust and its influence on marine biological activity in the South Atlantic Ocean. *Atmospheric Chemistry and Physics*, 11(6), 2487-2502.
- Johnson, M. S., Meskhidze, N., Solmon, F., Gassó, S., Chuang, P. Y., Gaiero, D. M., ... & Carouge, C. (2010). Modeling dust and soluble iron deposition to the South Atlantic Ocean. *Journal of Geophysical Research: Atmospheres*, 115(D15).
- Kedia, S., Kumar, R., Islam, S., Sathe, Y., & Kaginalkar, A. (2018). Radiative impact of a heavy dust storm over India and surrounding oceanic regions. *Atmospheric Environment*, 185, 109-120.
- Koffman, B. G., Goldstein, S. L., Winckler, G., Borunda, A., Kaplan, M. R., Bolge, L., ... & Vallelonga, P. (2021). New Zealand as a source of mineral dust to the atmosphere and ocean. *Quaternary Science Reviews*, 251, 106659.
- Kohfeld, K. E., & Harrison, S. P. (2001). DIRTMAP: the geological record of dust. *Earth-Science Reviews*, 54(1-3), 81-114.
- Kulshrestha, U. C., Reddy, L. A. K., Satyanarayana, J., & Kulshrestha, M. J. (2009). Real-time wet scavenging of major chemical constituents of aerosols and role of rain intensity in Indian region. *Atmospheric Environment*, 43(32), 5123-5127.

- Kumar, A., & Sarin, M. M. (2009). Mineral aerosols from western India: temporal variability of coarse and fine atmospheric dust and elemental characteristics. *Atmospheric Environment*, 43(26), 4005-4013.
- Kumar, A., Abouchami, W., Galer, S. J. G., Singh, S. P., Fomba, K. W., Prospero, J. M., & Andreae, M. O. (2018). Seasonal radiogenic isotopic variability of the African dust outflow to the tropical Atlantic Ocean and across to the Caribbean. *Earth and Planetary Science Letters*, 487, 94-105.
- Kumar, A., Suresh, K., & Rahaman, W. (2020). Geochemical characterization of modern aeolian dust over the Northeastern Arabian Sea: Implication for dust transport in the Arabian Sea. *Science of The Total Environment*, 729, 138576.
- Kumar, S. P., Madhupratap, M., Kumar, M. D., Gauns, M., Muraleedharan, P. M., Sarma, V. V. S. S., & De Souza, S. N. (2000). Physical control of primary productivity on a seasonal scale in central and eastern Arabian Sea. *Journal of Earth System Science*, 109, 433-441.
- Kumar, S. P., Ramaiah, N., Gauns, M., Sarma, V. V. S. S., Muraleedharan, P. M., Raghukumar, S., ... & Madhupratap, M. (2001). Physical forcing of biological productivity in the Northern Arabian Sea during the Northeast Monsoon. *Deep Sea Research Part II: Topical Studies in Oceanography*, 48(6-7), 1115-1126.
- Kumar, S. P., Roshin, R. P., Narvekar, J., Kumar, P. D., & Vivekanandan, E. (2010). What drives the increased phytoplankton biomass in the Arabian Sea?. *Current Science*, 101-106.
- Lee, C.M., Jones, B.H., Brink, K.H., Fischer, A.S., 2000. The upper-ocean response to monsoonal forcing in the Arabian Sea: Seasonal and spatial variability. *Deep Sea Res.: Part II* 47, 1177–1226. [https://doi.org/10.1016/S0967-0645\(99\)00141-1](https://doi.org/10.1016/S0967-0645(99)00141-1).
- Léon, J. F., & Legrand, M. (2003). Mineral dust sources in the surroundings of the north Indian Ocean. *Geophysical Research Letters*, 30(6).
- Li, J., Ren, Y., Zhang, F., Li, Y., Fang, Y., Wang, X., ... & Ye, Z. (2021). Contributions of Asian dust to subtropical soils of Southeast China based on Nd isotope. *Journal of Soils and Sediments*, 1-11.
- Measures, C. I., & Vink, S. (1999). Seasonal variations in the distribution of Fe and Al in the surface waters of the Arabian Sea. *Deep Sea Research Part II: Topical Studies in Oceanography*, 46(8-9), 1597-1622.
- Mills, M. M., Ridame, C., Davey, M., La Roche, J., & Geider, R. J. (2004). Iron and phosphorus co-limit nitrogen fixation in the eastern tropical North Atlantic. *Nature*, 429(6989), 292-294.
- Morel, F. M., Hudson, R. J., & Price, N. M. (1991). Limitation of productivity by trace metals in the sea. *Limnology and oceanography*, 36(8), 1742-1755.
- Morrison, J.M., Codispoti, L.A., Gaurin, S., Jones, B., Manghnani, V., Zheng, Z., 1998. Seasonal variation of hydrographic and nutrient fields during the US JGOFS Arabian Sea Process Study. *Deep Sea Res. Part II* 45 (10–11), 2053–2101. [https://doi.org/10.1016/S0967-0645\(98\)00063-0](https://doi.org/10.1016/S0967-0645(98)00063-0).

- Naqvi, S. W. A., Moffett, J. W., Gauns, M. U., Narvekar, P. V., Pratihary, A. K., Naik, H., ... & Ahmed, S. I. (2010). The Arabian Sea as a high-nutrient, low-chlorophyll region during the late Southwest Monsoon. *Biogeosciences*, 7(7), 2091-2100.
- Patra, P. K., Kumar, M. D., Mahowald, N., & Sarma, V. V. S. S. (2007). Atmospheric deposition and surface stratification as controls of contrasting chlorophyll abundance in the North Indian Ocean. *Journal of Geophysical Research: Oceans*, 112(C5).
- Patzert, W. C. (1974, February). Wind-induced reversal in Red Sea circulation. In *Deep Sea Research and Oceanographic Abstracts* (Vol. 21, No. 2, pp. 109-121). Elsevier.
- Paytan, A., Mackey, K. R., Chen, Y., Lima, I. D., Doney, S. C., Mahowald, N., ... & Post, A. F. (2009). Toxicity of atmospheric aerosols on marine phytoplankton. *Proceedings of the National Academy of Sciences*, 106(12), 4601-4605.
- Pease, P. P., Tchakerian, V. P., & Tindale, N. W. (1998). Aerosols over the Arabian Sea: geochemistry and source areas for aeolian desert dust. *Journal of Arid Environments*, 39(3), 477-496.
- Plocoste, T., Carmona-Cabezas, R., de Ravé, E. G., & Jimnez-Hornero, F. J. (2021). Wet scavenging process of particulate matter (PM10): A multivariate complex network approach. *Atmospheric Pollution Research*, 101095.
- Prenni, A. J., Petters, M. D., Kreidenweis, S. M., Heald, C. L., Martin, S. T., Artaxo, P., ... & Pöschl, U. (2009). Relative roles of biogenic emissions and Saharan dust as ice nuclei in the Amazon basin. *Nature Geoscience*, 2(6), 402-405.
- Rahaman, W., Lathika, N., Prabhat P., Tarique, M., Arya, K. S., Mishra, R., Thamban, M. (2023). Eolian versus fluvial supply to the northern Arabian Sea during the Holocene based on Nd isotope and geochemical records. *Geoscience Frontiers*, <https://doi.org/10.1016/j.gsf.2023.101618>
- Ramaswamy, V., Muraleedharan, P. M., & Babu, C. P. (2017). Mid-troposphere transport of Middle-East dust over the Arabian Sea and its effect on rainwater composition and sensitive ecosystems over India. *Scientific reports*, 7(1), 1-8.
- Rashki, A., Kaskaoutis, D. G., Mofidi, A., Minvielle, F., Chiapello, I., Legrand, M., ... & Francois, P. (2019). Effects of Monsoon, Shamal and Levar winds on dust accumulation over the Arabian Sea during summer—The July 2016 case. *Aeolian Research*, 36, 27-44.
- Rixen, T., Haake, B., & Ittekkot, V. (2000). Sedimentation in the western Arabian Sea the role of coastal and open-ocean upwelling. *Deep Sea Research Part II: Topical Studies in Oceanography*, 47(9-11), 2155-2178.
- Roesch, C., Roesch, M., Wolf, M. J., Zawadowicz, M. A., AlAloula, R., Awwad, Z., & Cziczo, D. J. (2021). CCN and INP activity of middle eastern soil dust. *Aeolian Research*, 52, 100729.
- Rojas, V. P., Meynadier, L., Colin, C., Bassinot, F., Valet, J. P., & Miska, S. (2019). Multi-tracer study of continental erosion and sediment transport to the Red Sea and the Gulf of Aden during the last 20 ka. *Quaternary Science Reviews*, 212, 135-148.

- Sauter, K., & L'Ecuyer, T. S. (2017). Observational evidence for the vertical redistribution and scavenging of Saharan dust by tropical cyclones. *Geophysical Research Letters*, *44*(12), 6421-6430.
- Scheuvens, D., Schütz, L., Kandler, K., Ebert, M., & Weinbruch, S. (2013). Bulk composition of northern African dust and its source sediments—A compilation. *Earth-Science Reviews*, *116*, 170-194.
- Seo, I., Lee, Y. I., Yoo, C. M., Kim, H. J., & Hyeong, K. (2014). Sr-Nd isotope composition and clay mineral assemblages in eolian dust from the central Philippine Sea over the last 600 kyr: Implications for the transport mechanism of Asian dust. *Journal of Geophysical Research: Atmospheres*, *119*(19), 11-492.
- Shinn, E. A., Smith, G. W., Prospero, J. M., Betzer, P., Hayes, M. L., Garrison, V., & Barber, R. T. (2000). African dust and the demise of Caribbean coral reefs. *Geophysical Research Letters*, *27*(19), 3029-3032.
- Singh, R. P., Prasad, A. K., Kayetha, V. K., & Kafatos, M. (2008). Enhancement of oceanic parameters associated with dust storms using satellite data. *Journal of Geophysical Research: Oceans*, *113*(C11).
- Sirocko, F. (1995). Abrupt changes in monsoon climate: evidences from the geochemical composition of Arabian Sea sediment, Habilitations Thesis, Univ. Kiel, Germany, 216.
- Sirocko, F., & Lange, H. (1991). Clay-mineral accumulation rates in the Arabian Sea during the late Quaternary. *Marine Geology*, *97*(1-2), 105-119.
- Sirocko, F., Garbe-Schönberg, D., & Devey, C. (2000). Processes controlling trace element geochemistry of Arabian Sea sediments during the last 25,000 years. *Global and Planetary Change*, *26*(1-3), 217-303.
- Skonieczny, C., Bory, A., Bout-Roumazelles, V., Abouchami, W., Galer, S. J. G., Crosta, X., ... & Ndiaye, T. (2013). A three-year time series of mineral dust deposits on the West African margin: sedimentological and geochemical signatures and implications for interpretation of marine paleo-dust records. *Earth and Planetary Science Letters*, *364*, 145-156.
- Stuut, J. B., Zabel, M., Rattmeyer, V., Helmke, P., Schefuß, E., Lavik, G., & Schneider, R. (2005). Provenance of present-day eolian dust collected off NW Africa. *Journal of Geophysical Research: Atmospheres*, *110*(D4).
- Suresh, K., Kumar, A., Ramaswamy, V., & Prakash Babu, C. (2021b). Seasonal variability in aeolian dust deposition fluxes and their mineralogical composition over the Northeastern Arabian Sea. *International Journal of Environmental Science and Technology*, 1-14.
- Suresh, K., Singh, U., Jha, A. K., Matta, V. M., Sudheer, A. K., & Kumar, A. (2022). Assessment of aeolian dust concentration, elemental composition, and their wet and dry deposition fluxes over the Northeast Arabian Sea. *Journal of the Air & Waste Management Association*, *72*(10), 1161-1173.

- Suresh, K., Singh, U., Kumar, A., Karri, D., Peketi, A., & Ramaswamy, V. (2021a). Provenance tracing of long-range transported dust over the Northeastern Arabian Sea during the southwest monsoon. *Atmospheric Research*, *250*, 105377.
- Svensson, A., Biscaye, P. E., & Grousset, F. E. (2000). Characterization of late glacial continental dust in the Greenland Ice Core Project ice core. *Journal of Geophysical Research: Atmospheres*, *105*(D4), 4637-4656.
- Tang, W., Yang, K., Qin, J., Li, X., & Niu, X. (2019). A 16-year dataset (2000–2015) of high-resolution (3 h, 10 km) global surface solar radiation. *Earth System Science Data*, *11*(4), 1905-1915.
- Teklay, M., Scherer, E. E., Mezger, K., & Danyushevsky, L. (2010). Geochemical characteristics and Sr–Nd–Hf isotope compositions of mantle xenoliths and host basalts from Assab, Eritrea: implications for the composition and thermal structure of the lithosphere beneath the Afar Depression. *Contributions to mineralogy and petrology*, *159*(5), 731-751.
- Tian, S., Liang, T., & Li, K. (2019). Fine road dust contamination in a mining area presents a likely air pollution hotspot and threat to human health. *Environment international*, *128*, 201-209.
- Tindale, N. W., & Pease, P. P. (1999). Aerosols over the Arabian Sea: Atmospheric transport pathways and concentrations of dust and sea salt. *Deep Sea Research Part II: Topical Studies in Oceanography*, *46*(8-9), 1577-1595.
- Tripathi, J. K., Bock, B., Rajamani, V., & Eisenhauer, A. (2004). Is river Ghaggar, Saraswati? geochemical constraints. *Current Science*, 1141-1145.
- Usher, C. R., Michel, A. E., & Grassian, V. H. (2003). Reactions on mineral dust. *Chemical reviews*, *103*(12), 4883-4940.
- Van Den Eeckhaut, M., Moeyersons, J., Nyssen, J., Abraha, A., Poesen, J., Haile, M., & Deckers, J. (2009). Spatial patterns of old, deep-seated landslides: A case-study in the northern Ethiopian highlands. *Geomorphology*, *105*(3-4), 239-252.
- Wang, S., Rao, W., Qian, J., Jin, K., Li, K., Feng, Y., & Zhao, J. (2021). Sr-Nd isotope and REE compositions of surface sediments from the three Gorges Reservoir: Implications for source identification and apportionment. *Journal of Hydrology*, *598*, 126279.
- Wang, Y., Peng, A., Chen, Z., Jin, X., & Gu, C. (2019). Transformation of gaseous 2-bromophenol on clay mineral dust and the potential health effect. *Environmental Pollution*, *250*, 686-694.
- Wiggert, J. D., & Murtugudde, R. G. (2007). The sensitivity of the southwest monsoon phytoplankton bloom to variations in aeolian iron deposition over the Arabian Sea. *Journal of Geophysical Research: Oceans*, *112*(C5).
- Xie, Y., Liu, L., Kang, C., & Chi, Y. (2020). Sr-Nd isotopic characteristics of the Northeast Sandy Land, China and their implications for tracing sources of regional dust. *Catena*, *184*, 104303.
- Xu, Z., Li, T., Clift, P. D., Lim, D., Wan, S., Chen, H., ... & Xiong, Z. (2015). Quantitative estimates of Asian dust input to the western Philippine Sea in the mid-late Quaternary and its potential significance for paleoenvironment. *Geochemistry, Geophysics, Geosystems*, *16*(9), 3182-3196.



- Yadav, S., & Rajamani, V. (2004). Geochemistry of aerosols of northwestern part of India adjoining the Thar Desert. *Geochimica et Cosmochimica Acta*, 68(9), 1975-1988.
- ZHANG, X. (1996). Elemental tracers for Chinese source dust. *Science in China (series D)*, 39, 512-521.
- Zhao, R., Han, B., Lu, B., Zhang, N., Zhu, L., & Bai, Z. (2015). Element composition and source apportionment of atmospheric aerosols over the China Sea. *Atmospheric Pollution Research*, 6(2), 191-201.

**Table 1:** Sample ID, date of collection,  $^{87}\text{Sr}/^{86}\text{Sr}$ ,  $^{143}\text{Nd}/^{144}\text{Nd}$  and  $\epsilon_{\text{Nd}}$  values, relative percentages (%) of smectite (S), palygorskite (P), illite (I), chlorite (C) and kaolinite (K) as well as I/K and K/C.

Sample id	Date of collection	$^{87}\text{Sr}/^{86}\text{Sr}$	$\pm 2\sigma$	$^{143}\text{Nd}/^{144}\text{Nd}$	$\pm 2\sigma$	$\epsilon_{\text{Nd}}$	Weighted peak area percentage					I/K	K/C
							S	P	I	K	C		
WDP 14-1	2-3 JUN2014	0.713631	9	0.512318	16	-6.4	9	8	42	16	24	2.6	0.7
WDP 14-2	14-15 JUN 2014	0.712043	10	0.512399	34	-4.8	9	12	44	15	20	2.9	0.8
WDP 14-3	16-17 JUN 2014	0.711522	9	0.512406	16	-4.7	16	12	28	19	24	1.5	0.8
WDP 14-4	21-26 JUN 2014	0.712595	8	0.512335	14	-6.1	9	31	22	15	22	1.4	0.7
WDP 14-5	8-9 JUL 2014	0.711478	9	0.512361	16	-5.5	16	37	18	15	15	1.2	1
WDP 14-6	13-14 JUL 2014	0.71115	9	0.512441	13	-4	16	39	17	13	16	1.3	0.8
WDP 14-7	19-20 JUL 2014	0.710853	10	0.512434	18	-4.1	29	14	18	18	21	1	0.8
WDP 14-8	22-23 JUL 2014	0.709916	9	0.512490	15	-3	27	16	26	14	19	1.9	0.7
WDP 14-9	30-31 JUL 2014	0.71313	8	0.512358	16	-5.6	20	20	31	15	15	2.1	1
WDP 14-10	4-5 AUG 2014	0.711182	9	0.512382	17	-5.1	27	20	25	12	28	2	0.4
WDP 14-11	7-8 AUG 2014	0.710107	10	0.512470	20	-3.4	27	11	22	18	22	1.2	0.8
WDP 14-12	11-12 AUG 2014	0.711107	9	0.512425	13	-4.2	26	13	18	20	24	0.9	0.9
WDP 14-13	26-27 AUG 2014	0.713142	10	0.512351	31	-5.7	16	ND	37	18	29	2	0.6
WDP 14-14	4-5 SEP 2014	0.714679	10	0.512343	20	-5.8	*ND	ND	ND	ND	ND	ND	ND
WDP 14-15	13-14 SEP 2014	0.713534	8	0.512419	27	-4.3	ND	ND	ND	ND	ND	ND	ND
WDP 15-2	8-9 JUN 2015	0.718262	25	ND		ND	ND	ND	ND	ND	ND	ND	ND
WDP 15-3	21-22 JUN 2015	0.712513	17	ND		ND	23	25	19	14	16	1.3	0.9
WDP 15-4	25-26 JUN 2015	0.712406	9	0.512415	29	-4.4	21	36	19	9	14	2.1	0.6
WDP 15-5	30 JUN-2 JUL 2015	0.71131	11	0.512419	27	-4.3	29	13	22	18	16	1.2	1.2
WDP 15-6	8-9 JUL 2015	0.71318	12	0.512546	22	-1.9	23	19	29	8	19	3.6	0.4
WDP 15-7	15-16 JUL 2015	0.711422	13	0.512453	26	-3.7	34	20	25	11	9	2.2	1.3
WDP 15-8	21-22 JUL 2015	0.713092	15	0.512366	36	-5.2	24	ND	51	ND	24	ND	ND
WDP 15-9	26-27 JUL 2015	0.713035	16	0.512473	40	-3.4	19	26	29	9	15	3.3	0.6

WDP 15-10	31 JUL - 1 AUG 2015	0.711297	12	0.512617	29	-0.6	32	16	22	15	14	1.4	1.1
WDP 15-11	6-7 AUG 2015	0.71099	16	0.512494	45	-2.9	42	10	18	12	16	1.4	0.8
WDP 15-12	12-13 AUG 2015	0.711563	11	0.512400	14	-4.9	28	8	35	16	12	2.1	1.3
WDP 15-13	16-17 AUG 2015	0.711646	9	0.512452	25	-3.8	32	17	21	13	15	1.6	0.9
WDP 15-14	28-30 AUG 2015	0.713337	9	0.512390	21	-5.1	15	26	29	11	18	2.8	0.6
WDP 15-15	12-14 SEP 2015	0.717726	11	0.512337	27	-6.1	9	ND	52	14	22	3.8	0.6
WDP 15-16	18-20 SEP 2015	0.719305	9	0.512203	27	-8.7	ND	ND	56	ND	40	ND	ND
WDP 19-1	12-18 JUL 2019	0.710641	11	0.512472	13	-3.4	33	22	17	13	14	1.3	0.9
WDP 19-2	18-19 JUL 2019	0.711009	9	0.512444	34	-3.9	32	21	18	15	13	1.2	1.1
WDP 19-3	19-24 JUL 2019	0.71249	8	0.512373	18	-5.3	29	16	21	18	13	1.2	1.4
WDP 19-4	26-29 JUL 2019	0.711596	8	0.512446	17	-3.8	32	16	25	13	13	1.9	1
WDP 19-5	29-31 JUL 2019	0.711821	9	0.512505	17	-2.5	27	17	25	12	16	2.1	0.8
WDP 19-6	31 JUL - 6 AUG 2019	0.711851	11	0.512412	38	-4.4	11	16	31	19	21	1.7	0.9
WDP 19-7	6-9 AUG 2019	0.71163	10	0.512394	15	-4.7	9	17	32	13	27	2.4	0.5
WDP 19-8	9-13 AUG 2019	0.71099	10	0.512414	21	-4.3	11	32	21	15	18	1.4	0.8
WDP 19-9	13-19 AUG 2020	0.711586	10	0.512394	26	-4.7	28	16	24	13	17	1.8	0.8
WDP 19-10	19-23 AUG 2019	0.712041	11	0.512414	21	-4.3	28	15	28	12	15	2.3	0.8
WDP 19-11	23-29 AUG 2019	0.711618	9	0.512408	14	-4.4	29	12	27	17	13	1.5	1.3
WDP 19-12	29 AUG-3 SEP 2019	0.712489	8	ND		ND	31	5	25	19	19	1.3	1
WDP 19-13	3-6 SEP 2019	0.712583	10	0.512529	20	-2.1	21	ND	49	13	16	3.9	0.8
WDP 19-14	6-12 SEP 2019	0.71271	9	0.512387	18	-4.9	11	25	29	14	19	2.1	0.7

\*ND: not detected

**Table 2a:** Trace metals concentration (Major elements data mentioned in Suresh et. al., 2021a) of the wet deposited dust samples collected during the SWM period of 2013.

<b>Sample ID</b>	<b>WDP 13-1</b>	<b>WDP 13-2</b>	<b>WDP 13-3</b>	<b>WDP 13-4</b>	<b>WDP 13-5</b>	<b>WDP13-6</b>	<b>WDP 13-7</b>	<b>WDP 13-8</b>	<b>WDP 13-9</b>	<b>WDP 13-10</b>	<b>WDP 13-11</b>	<b>WDP 13-12</b>	<b>WDP 13-13</b>	<b>WDP 13-14</b>	<b>WDP 13-15</b>	<b>WDP 13-16</b>
ppm																
<b>Cu</b>	68.5	50.8	85.7	71.2	101.1	90.2	101.8	91.7	76.1	78.2	69.6	129.2	139.3	236.4	105.3	97.4
<b>Co</b>	31.7	26.6	27.0	28.3	31.2	36.2	35.2	35.5	28.7	33.5	27.0	39.6	33.9	17.6	21.4	24.4
<b>Mn</b>	726.0	760.9	602.2	706.0	848.6	861.1	878.7	1077.7	675.9	846.7	731.6	1194.8	981.1	511.1	488.2	625.2
<b>V</b>	168.4	122.1	168.7	160.7	172.8	205.0	203.0	201.5	174.3	174.0	153.5	237.5	230.7	153.0	160.7	159.8
<b>Rb</b>	15.7	12.5	18.7	11.2	39.7	17.6	62.4	10.9	11.1	7.9	10.2	25.4	26.2	63.5	32.7	11.7
<b>Sr</b>	87.1	79.1	88.6	90.8	121.8	85.8	142.2	101.2	58.5	86.2	78.2	149.0	138.1	92.1	82.6	88.7
<b>Th</b>	3.7	3.5	3.4	2.2	5.8	3.5	7.7	3.0	2.5	1.6	1.9	3.2	4.8	10.0	4.2	3.3
<b>U</b>	2.7	2.9	2.8	2.4	2.8	2.9	3.2	2.1	2.1	2.3	2.1	3.7	3.5	4.7	3.1	2.6
<b>Cd</b>	1.0	0.6	1.1	0.9	0.8	0.9	1.0	0.7	0.6	0.7	0.8	1.3	0.9	3.6	1.4	1.3
<b>Nd</b>	11.7	11.0	9.0	8.0	19.6	10.9	24.9	11.5	7.5	6.5	5.5	12.3	12.2	28.2	8.4	8.4
<b>Sm</b>	2.6	2.5	1.6	1.7	4.0	2.4	4.8	2.7	1.7	1.4	1.1	2.3	2.5	3.1	1.5	1.8

**Table 2b:** Major elements and trace metals concentration of the wet deposited dust samples collected during the SWM period of 2014.

<b>Sample ID</b>	<b>WDP 14-1</b>	<b>WDP 14-2</b>	<b>WDP 14-3</b>	<b>WDP 14-4</b>	<b>WDP 14-5</b>	<b>WDP 14-6</b>	<b>WDP 14-7</b>	<b>WDP 14-8</b>	<b>WDP 14-9</b>	<b>WDP 14-10</b>	<b>WDP 14-11</b>	<b>WDP 14-12</b>	<b>WDP 14-13</b>	<b>WDP 14-14</b>	<b>WDP 14-15</b>
%															
<b>Al</b>	7.9	8.2	8.3	5.9	5.1	7.6	7.6	7.6	8	7.1	7.3	7.2	7.3	7.6	7.3
<b>Ca</b>	0.6	0.7	0.7	1.1	1.3	0.7	0.8	0.9	0.6	0.7	0.7	0.7	0.5	0.7	0.7
<b>Mg</b>	2.6	2.9	2.5	2.9	3.4	2.4	2.6	2.7	2.5	2.2	2.2	2.2	2.7	1.7	3.5
<b>Fe</b>	5.5	5.5	5.7	4.1	3.4	5.5	5.9	6	5	5.4	5	5.2	4.9	4.8	4.9
<b>Ti</b>	0.6	0.6	0.6	0.4	0.4	0.6	0.7	0.7	0.6	0.6	0.6	0.5	0.5	0.5	0.5
ppm															
<b>Cu</b>	104.2	95.0	93.0	74.1	62.8	111.7	112.4	91.3	90.4	93.7	86.4	114.2	227.7	101.9	131.8
<b>Co</b>	23.6	30.4	26.7	22.9	21.4	27.6	37.5	31.5	26.1	26.9	26.3	27.3	23.0	22.9	26.4
<b>Mn</b>	813.0	846.7	823.2	782.0	625.5	925.4	902.3	880.8	922.4	868.3	839.8	877.7	633.6	651.6	953.2
<b>V</b>	171.1	181.4	166.1	129.6	108.4	171.3	212.7	180.2	170.7	163.8	154.6	158.9	154.2	153.8	159.3
<b>Rb</b>	64.3	52.4	56.3	42.2	27.8	54.3	25.1	23.3	63.1	23.2	40.0	46.9	77.3	85.2	87.6
<b>Sr</b>	118.0	152.2	126.5	98.9	90.0	132.8	156.9	128.3	122.9	109.3	117.5	117.6	95.9	108.3	118.7
<b>Th</b>	10.6	10.4	10.1	7.3	5.6	9.6	8.8	7.3	10.6	7.7	7.9	9.6	10.2	12.0	11.4
<b>U</b>	3.0	3.3	2.9	2.6	2.3	2.9	3.2	2.5	3.0	2.4	2.3	2.8	3.0	2.8	3.1
<b>Cd</b>	0.7	0.7	0.6	0.6	0.6	1.5	0.8	0.7	0.7	0.6	0.6	0.8	1.3	1.0	1.2
<b>Nd</b>	31.0	30.7	33.9	21.1	19.2	32.3	33.7	29.7	29.0	27.6	29.3	33.0	29.1	31.2	30.9
<b>Sm</b>	6.5	6.6	7.3	4.3	4.1	6.6	7.7	6.6	6.2	6.2	6.5	7.1	5.6	6.4	6.3

**Table 2c:** Major elements and trace metals concentration of the wet deposited dust samples collected during the SWM period of 2015.

<b>Sample ID</b>	<b>WDP 15-3</b>	<b>WDP 15-4</b>	<b>WDP 15-5</b>	<b>WDP 15-6</b>	<b>WDP 15-7</b>	<b>WDP 15-8</b>	<b>WDP 15-9</b>	<b>WDP 15-10</b>	<b>WDP 15-11</b>	<b>WDP 15-12</b>	<b>WDP 15-13</b>	<b>WDP 15-14</b>	<b>WDP 15-15</b>	<b>WDP 15-16</b>
%														
<b>Al</b>	7.6	7	9	8	8.1	8.6	8.5	8.5	8.5	8.3	8.4	7.9	4.5	7.5
<b>Ca</b>	0.6	1.5	1	0.6	0.8	0.6	0.6	0.8	0.8	0.7	0.8	0.6	0.5	0.5
<b>Mg</b>	3.2	4.3	3.2	2.8	2.8	2.8	2.9	2.6	2.9	2.7	2.7	2.4	1	2.1
<b>Fe</b>	4.8	4.6	6.5	5.2	5.9	5.5	5.7	5.9	6	5.6	6	5.3	4.3	4.6
<b>Ti</b>	0.5	0.4	0.7	0.6	0.6	0.5	0.6	0.7	0.7	0.6	0.7	0.6	0.4	0.5
ppm														
<b>Cu</b>	86.5	96.7	117.1	94.2	98.0	87.9	94.9	105.0	108.9	95.3	98.9	99.4	170.4	91.2
<b>Co</b>	25.7	28.0	32.2	27.2	30.8	26.2	26.4	28.0	30.6	30.1	29.6	23.1	16.7	23.0
<b>Mn</b>	685.9	903.2	922.5	790.8	888.5	794.4	833.2	888.2	892.0	1038.1	920.2	698.9	451.6	643.4
<b>V</b>	142.2	142.3	185.0	161.8	175.2	161.8	167.6	172.3	181.5	173.7	171.5	154.5	131.7	154.7
<b>Rb</b>	78.3	67.0	48.9	52.1	40.2	77.4	64.9	45.1	42.8	66.3	55.8	56.8	48.2	86.7
<b>Sr</b>	107.1	110.1	148.2	112.0	118.0	120.2	113.1	118.2	120.2	125.0	116.5	98.9	83.6	100.4
<b>Th</b>	9.8	8.7	10.8	10.2	8.8	10.5	10.9	9.7	10.0	10.5	10.5	10.1	7.3	10.4
<b>U</b>	2.8	2.7	3.2	3.0	2.7	2.8	3.0	2.8	2.9	3.0	2.9	2.8	4.5	3.0
<b>Cd</b>	0.8	1.1	0.9	0.7	0.9	0.7	0.7	0.8	0.8	0.8	0.8	1.0	1.2	2.0
<b>Nd</b>	30.4	24.7	39.0	30.2	32.4	29.8	33.3	34.3	35.0	33.7	36.2	31.8	20.9	26.4
<b>Sm</b>	6.4	5.4	8.3	6.5	7.0	6.4	6.8	7.2	7.6	7.1	7.7	6.6	4.2	5.3

**Table 2d:** Major elements and trace metals concentration of the wet deposited dust samples collected during the SWM period of 2019.

<b>Sample ID</b>	<b>WDP 19-1</b>	<b>WDP 19-2</b>	<b>WDP 19-3</b>	<b>WDP 19-4</b>	<b>WDP 19-5</b>	<b>WDP 19-6</b>	<b>WDP 19-7</b>	<b>WDP 19-8</b>	<b>WDP 19-9</b>	<b>WDP 19-10</b>	<b>WDP 19-11</b>	<b>WDP 19-12</b>	<b>WDP 19-13</b>	<b>WDP 19-14</b>
%														
<b>Al</b>	4.3	4.6	4	4.5	4.2	5.5	4.9	4.8	4.8	4.6	4.9	4.7	5.2	4.2
<b>Ca</b>	0.5	0.5	0.3	0.4	0.3	0.5	0.6	0.6	0.5	0.4	0.5	0.3	0.4	0.3
<b>Mg</b>	1.5	1.4	1.1	1.4	1.1	1.7	1.9	2	1.8	1.4	1.3	1.2	1.5	1.2
<b>Fe</b>	4	4.8	3.8	4	3.8	4.2	4	3.9	4	4.1	3.7	3.8	3.8	3.9
<b>Ti</b>	0.5	0.5	0.5	0.5	0.4	0.5	0.5	0.5	0.5	0.5	0.4	0.5	0.5	0.5
ppm														
<b>Cu</b>	75.9	161.4	132.6	75.2	66.4	63.6	67.7	57.4	85.5	69.5	78.8	63.8	81.4	65.6
<b>Co</b>	20.9	21.4	21.5	22.3	17.8	19.7	25.7	22.5	29.1	22.7	22.6	20.4	24.7	20.4
<b>Mn</b>	607.2	562.1	598.5	608.4	502.0	546.7	697.9	696.5	863.9	675.2	825.7	649.5	704.1	651.0
<b>V</b>	127.3	150.3	150.8	138.0	120.2	129.6	149.8	128.2	163.4	140.7	134.5	127.9	163.3	137.4
<b>Rb</b>	11.0	12.8	13.3	12.3	14.1	23.9	21.6	20.0	19.6	19.1	18.9	17.9	29.4	18.7
<b>Sr</b>	82.9	89.5	93.5	84.8	79.0	92.3	108.6	101.3	113.2	87.1	100.8	80.8	109.4	73.8
<b>Th</b>	3.4	2.6	3.7	3.7	2.7	5.0	4.6	5.1	5.0	3.6	4.9	4.0	7.3	3.1
<b>U</b>	1.8	1.9	2.3	2.1	1.9	2.2	2.5	2.4	2.7	2.3	2.7	2.2	2.9	2.3
<b>Cd</b>	0.7	0.5	0.6	0.6	0.6	0.5	0.6	0.5	0.6	0.6	1.0	0.6	0.6	0.7
<b>Nd</b>	12.6	9.2	12.7	10.4	8.7	14.6	13.2	17.2	14.3	10.7	13.9	10.1	19.2	9.9
<b>Sm</b>	2.8	1.9	2.5	2.3	1.7	3.2	2.8	3.7	3.1	2.2	3.1	2.2	4.2	2.1

**Table 3:** Sr and Nd isotopic composition and concentration of four end-members defined as the Arabian Peninsula, SW Asia, the NE Africa and Thar desert.

<b>End members</b>	<b><math>^{87}\text{Sr}/^{86}\text{Sr}</math></b>	<b>Std. dev.</b>	<b>Sr conc. (ppm)</b>	<b><math>\epsilon_{\text{Nd}}</math></b>	<b>Std dev.</b>	<b>Nd conc. (ppm)</b>	<b>References</b>
Arabian Peninsula	0.7122	0.003	750	- 6.6	1.5	20	Kumar et al. (2020); Sirocko (1995)
SW Asia	0.7124	0.006	107	- 11.9	3.8	12	Kumar et al. (2020)
NE Africa	0.7046	0.0004	574	1.7	1.1	32	Ayalew et al. (2018)
Thar desert	0.7350	0.006	300	- 13.9	1.4	35	Tripathi et al. (2004), Ferrat et al. (2011)



**Figure 1a:** Map showing CALIPSO profile, air mass back trajectories, and average UV-aerosol index over source region during the sampling period of 2014 for WDP samples (i) WDP 14-2 (ii) WDP 14-8 and (iii) WDP 14-14 collected at beginning, mid and end of the SWM respectively

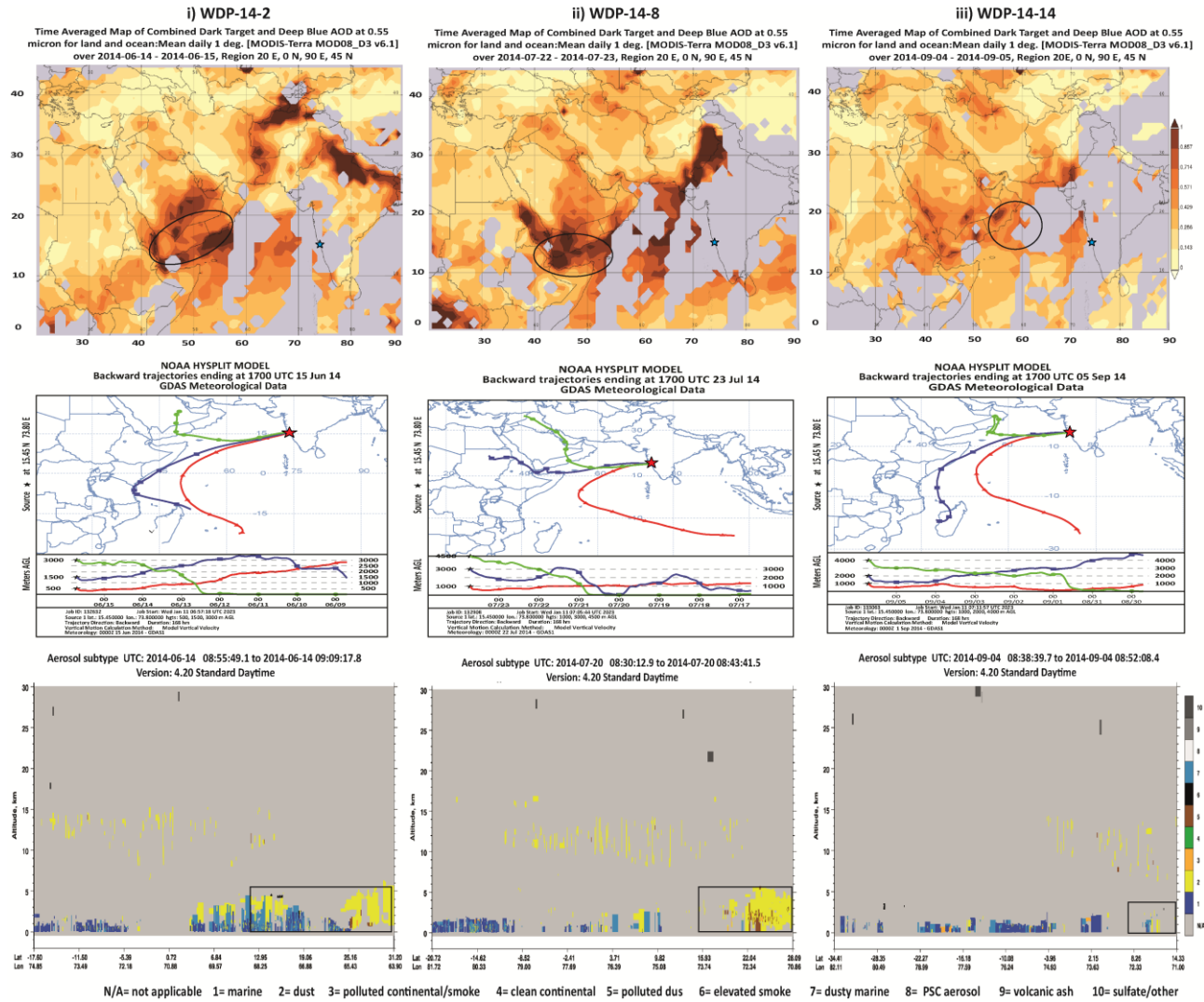


**Figure 1b:** Map showing CALIPSO profile, air mass back trajectories, and average UV-aerosol index over source region during the sampling period of 2015 for WDP samples (i) WDP 15-4 (ii) WDP 15-9 and (iii) WDP 15-16 collected at beginning, mid and end of the SWM respectively.

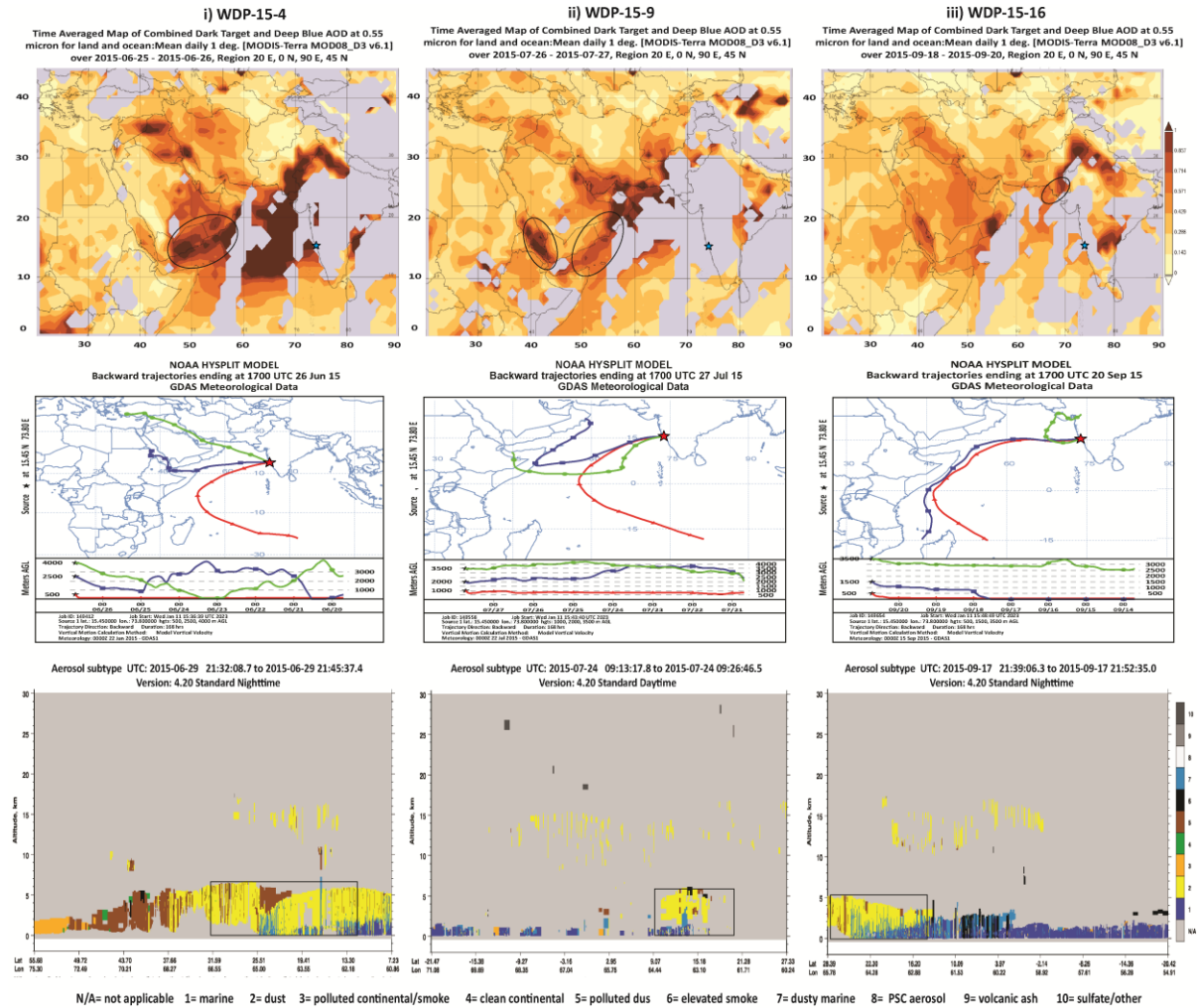


**Figure 1c:** Map showing CALIPSO profile, air mass back trajectories, and average UV-aerosol index over source region during the sampling period of 2019 for WDP samples (i) WDP 19-5 and (ii) WDP 19-13 collected at mid and end of the SWM respectively.

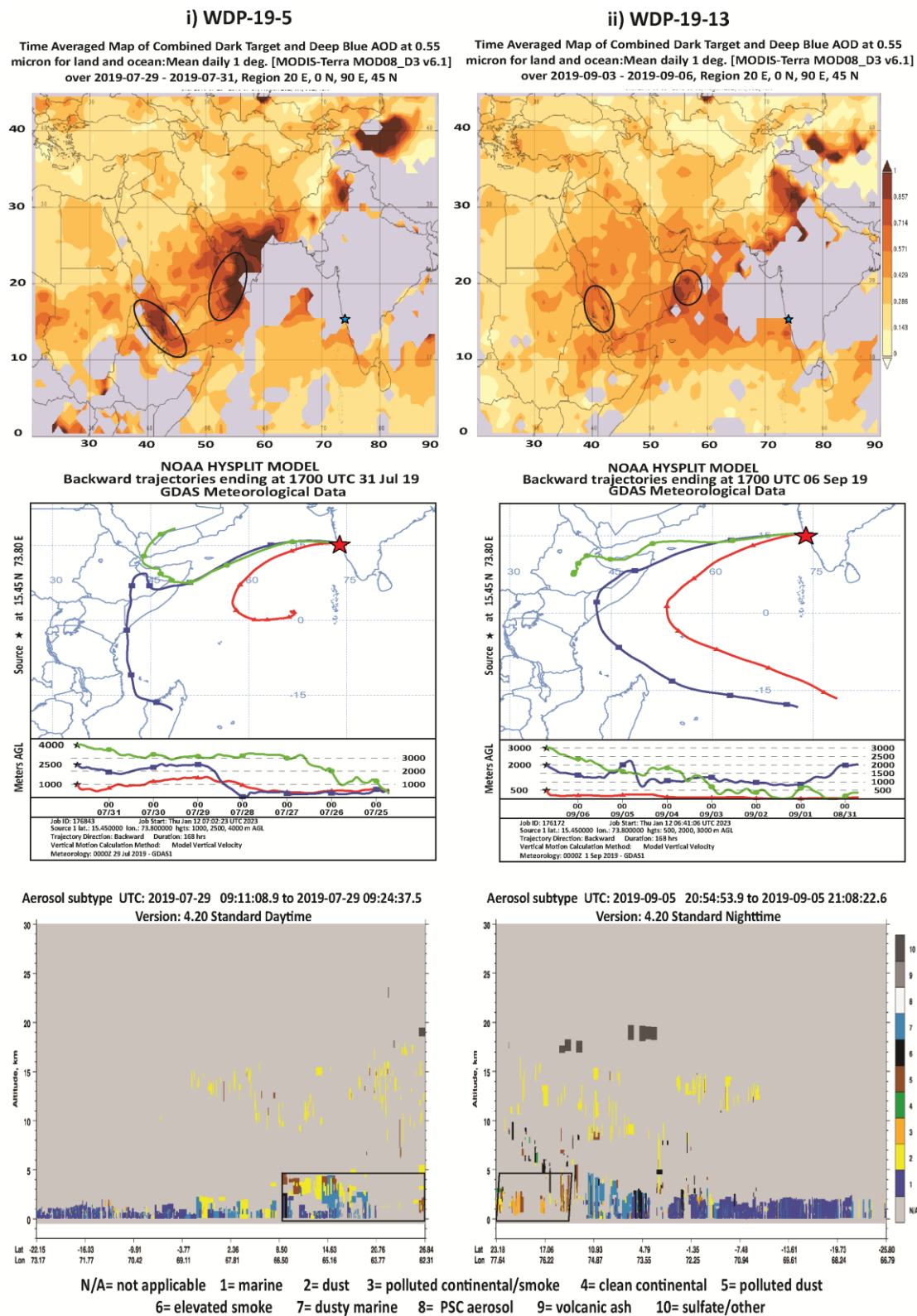


**Figure 2:** Temporal variation in abundance of palygorskite and smectite as well as illite/kaolinite and kaolinite/chlorite ratio.

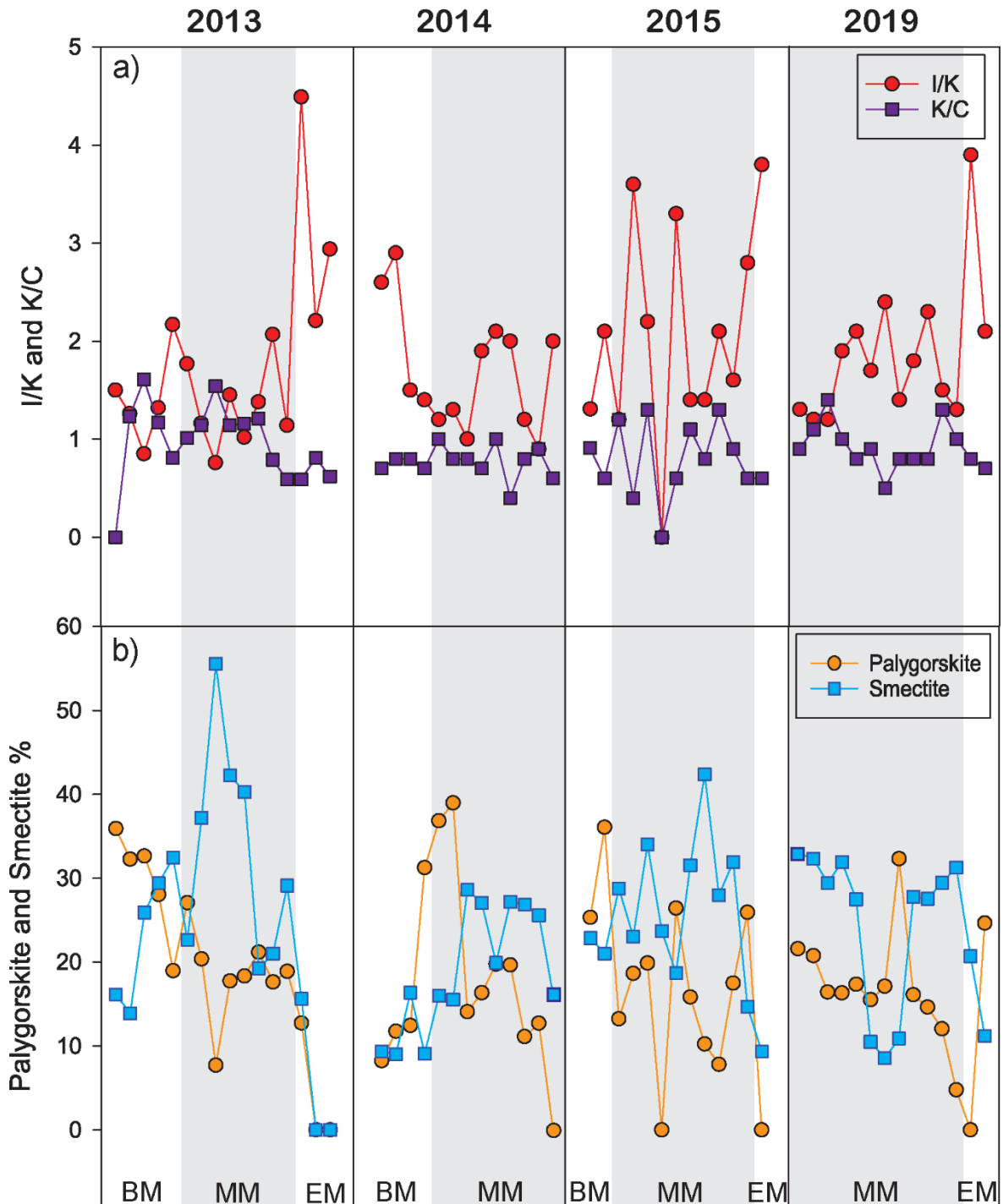


**Figure 3:** Variation in the isotopic composition (Sr and Nd) of dust reaching to the NEAS during SWM period of 2013 (published, Suresh et al., 2013), 2014, 2015 and 2019.

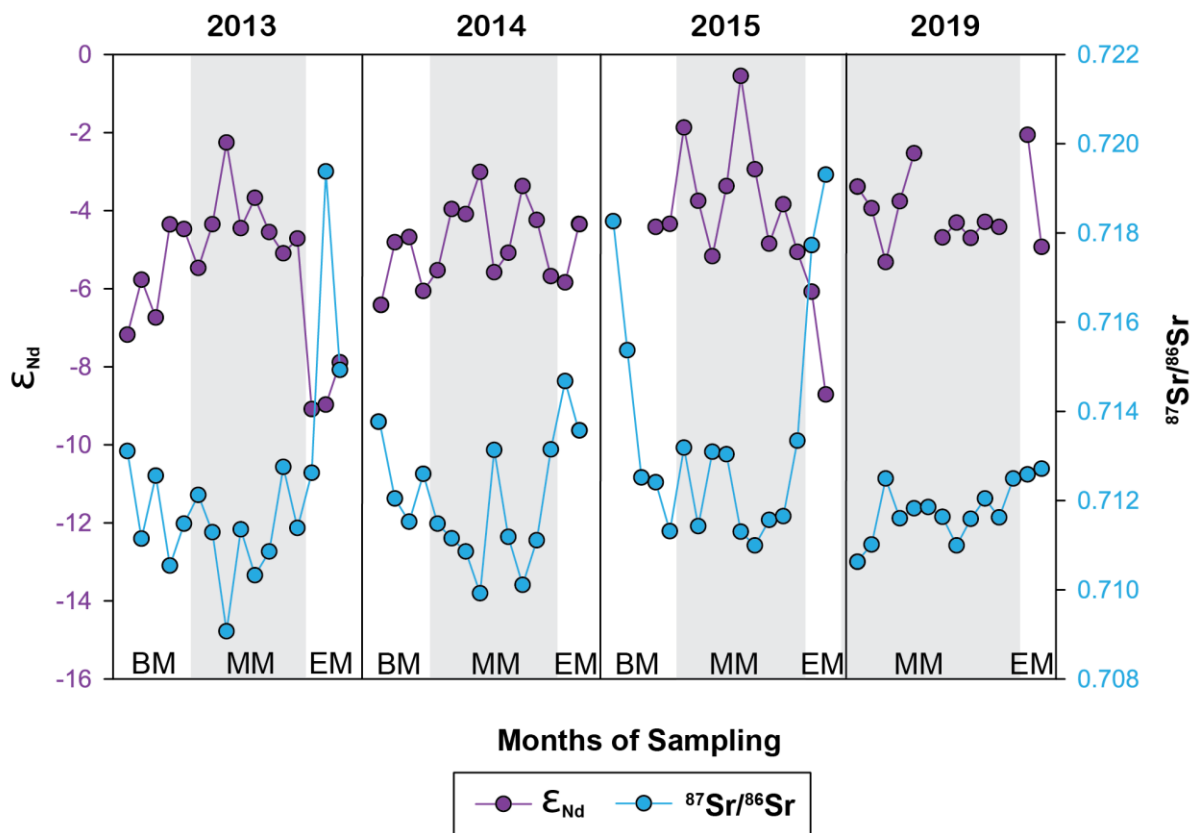


**Figure 4:** Sr vs. Nd isotopic compositions of the WDP samples (2013-15 and 2019, altogether characterized as BM, MM, EM) plotted along with potential source region isotopic fields inferred from the literature data (Table 3). Mixing line between ARB and NEA, SWA, and Thar Desert are also shown.

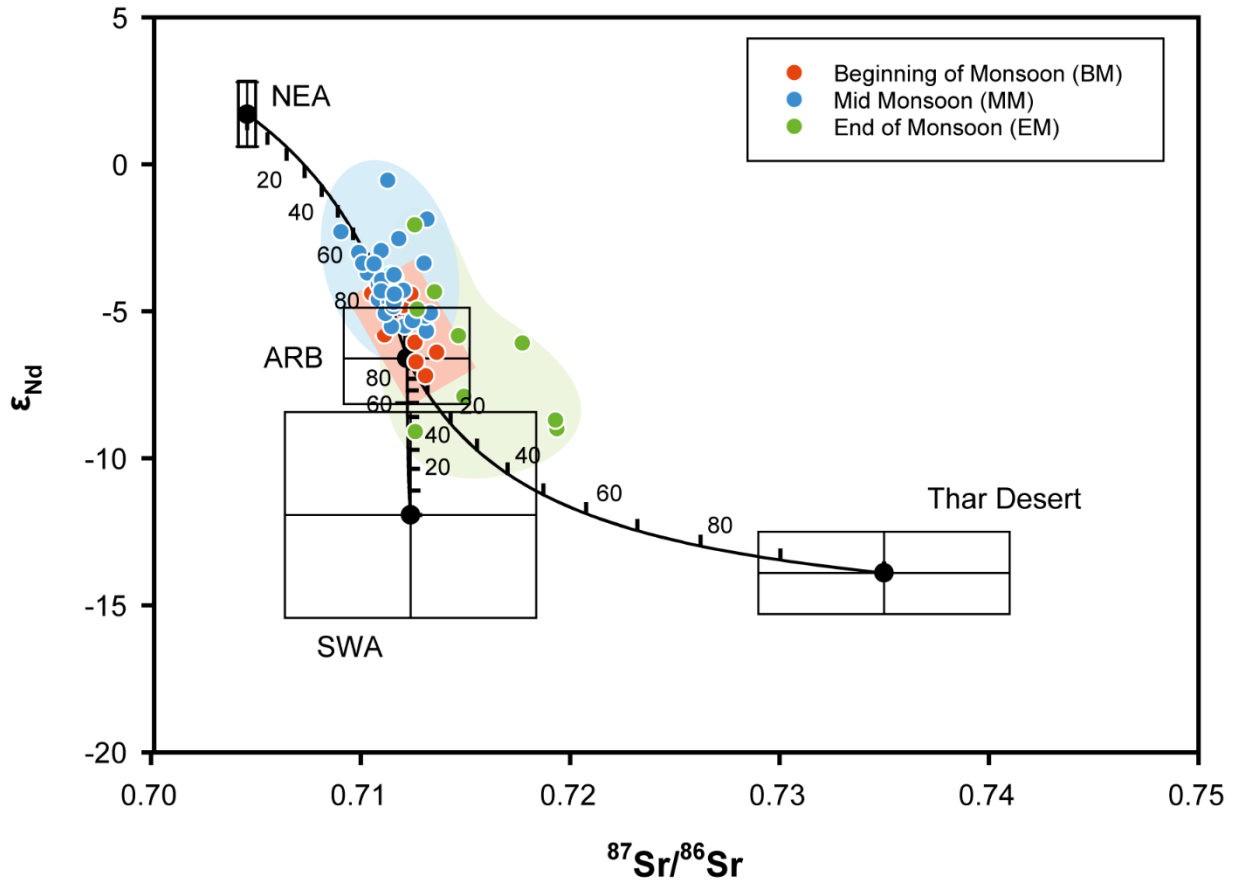


**Figure 5:** Variation in the Smectite content with  $\epsilon_{Nd}$  value in the samples collected during BM, MM and EM period of 2013-15 and 2019 (refer text for more detail on source nomenclature).

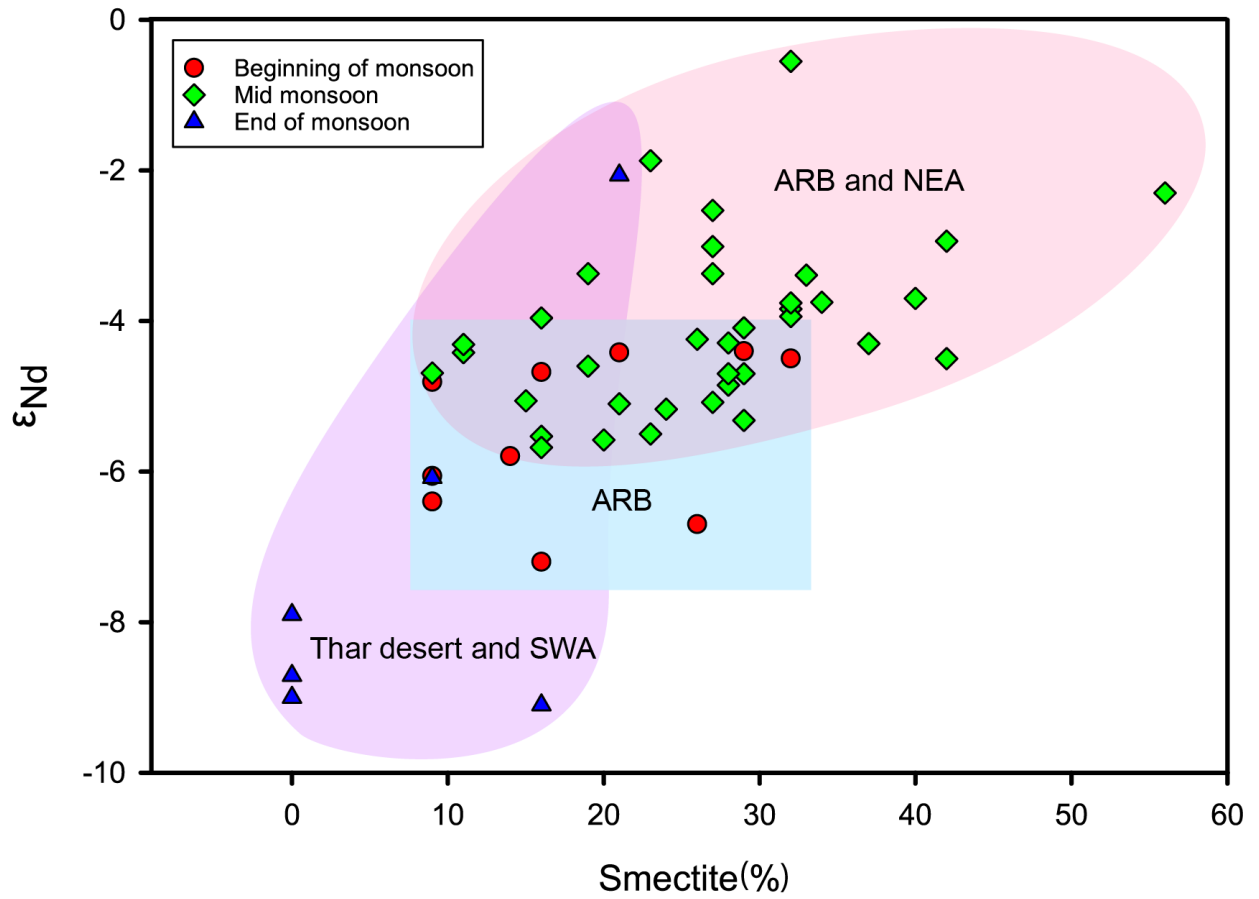


**Figure 6:** Variation of trace metals (Cu, Fe and Mn) concentrations in WDP samples with  $\epsilon_{Nd}$  for identified dust sources viz. Arabian Peninsula, mix of Arabian Peninsula and NE Africa, Southwest Asia and Thar desert.

